

Evaluation of transport in stratospheric models

Timothy M. Hall,¹ Darryn W. Waugh,² Kristie A. Boering,³ R. Alan Plumb⁴

Abstract. We evaluate transport characteristics of two- and three-dimensional chemical transport models of the stratosphere by comparing their simulations of the mean age of stratospheric air and the propagation of annually periodic oscillations in tracer mixing ratio at the tropical tropopause into the stratosphere to inferences from in situ and satellite observations of CO₂, SF₆, and water vapor. The models, participants in the recent NASA “Models and Measurements II” study, display a wide range of performance. Most models propagate annual oscillations too rapidly in the vertical and overattenuate the signal. Most models also significantly underestimate mean age throughout the stratosphere, and most have at least one of several unrealistic features in their mean age contour shapes. In the lower stratosphere, model-to-model variation in N₂O, NO_y, and Cl_y is well correlated with variation in mean age, and the magnitude of NO_y and Cl_y variation is large. We conclude that model transport inaccuracies significantly affect simulations of important long-lived chemical species in the lower stratosphere.

1. Introduction

The environmental impact of anthropogenic pollutants on the stratosphere is determined by a complex interaction among chemistry, radiation, and transport. In order to predict future chemical and climate changes due to such pollutants, models must include these processes. However, in order to assess the realism of models, and therefore to know what weight to give model predictions, it is preferable to evaluate components of models separately, so that the causes of any unrealistic features may be better isolated. In this paper, we evaluate transport in a range of stratospheric models by performing simulations of chemically inert tracers and comparing the results to previously published and new observations.

This study summarizes a component of the recent “Models and Measurements 2” (MM2) stratospheric model intercomparison [Park *et al.*, 1999]. MM2 follows the 1992 MM intercomparison [Prather and Remsberg, 1993] and has been performed not only because of changes in models in the intervening 6 years, but also

because a large amount of new data is now available from satellite, aircraft, and balloon platforms against which to evaluate model results. In particular, MM models performed only one pure transport experiment, bomb radiocarbon, for which observed data are sparse. However, we now have high precision measurements in the lower stratosphere at most latitudes and seasons, and some measurements in the middle stratosphere, of nearly inert tracers such as CO₂ and SF₆ from several in situ campaigns in recent years. In addition, we have a multiyear time series of $\dot{H} = \text{H}_2\text{O} + 2\text{CH}_4$, a quasi-conserved tracer providing much information about tropical transport, from the Halogen Occultation Experiment (HALOE) instrument aboard the Upper Atmosphere Research Satellite (UARS). These observations comprise a powerful set of data, which reveals inaccuracies in model transport.

MM2 defined six transport experiments: (1) the age spectrum, (2) idealized tracers with annually periodic surface boundary conditions (sine and cosine), (3) SF₆, (4) CO₂, (5) inert tracers of proposed stratospheric high speed civil transport (HSCT) aircraft emissions, and (6) inert tracers of HSCT emissions north of 40°N. See Table 1 for details of the experiments discussed here. These six different simulations do not provide mutually independent information. For example, as we will show, much information of interest from the periodic boundary condition, SF₆, and CO₂ experiments is contained in the age spectrum. Thus, in this paper, we focus mainly on simulations of the age spectrum. The simulations of HSCT emission tracers and their relationship to other tracers will be presented elsewhere. See Park *et al.* [1999] for more details.

In section 2 we briefly introduce participating models, while in section 3 we present model simulations of the age spectrum and illustrate how observable tracers

¹NASA Goddard Institute for Space Studies, New York, New York.

²Department of Earth and Planetary Sciences, Johns Hopkins University, Baltimore, Maryland.

³Department of Geology and Geophysics and Department of Chemistry, University of California, Berkeley.

⁴Department of Earth, Atmospheric, and Planetary Sciences, Massachusetts Institute of Technology, Cambridge.

Copyright 1999 by the American Geophysical Union.

Paper number 1999JD900226.
0148-0227/99/1999JD900226\$09.00

Table 1. Details of the Experiments

Experiment	Initial Condition	Boundary Condition
Age spectrum	0 everywhere	Within zonal band $\pm 10^\circ$ and surface to 2 km, mixing ratio held 1 for January, then 0 for rest of 20 year run. No-flux elsewhere.
Sin tracer	1 everywhere	Same region as age spectrum; time dependence is $1 + \sin(2\pi t/1 \text{ year})$
Cos tracer	1 everywhere	Same as sin tracer, but $1 + \cos(2\pi t/1 \text{ year})$
SF ₆	0 everywhere	Flux into surface layer 30° to 60° N, uniform per unit area, with steady increase such that total kilotons released during year t is $0.2(t - 1966)$. Run from $t = 1966$ to 2000.

may be reconstructed from the age spectrum. Section 4 focuses on the global mean age distribution, making comparisons to observations, identifying components of model transport that have strong leverage over mean age, and discussing similarities of mean age variations to variations of other long-lived trace gases. Model transport in the tropics is analyzed in section 5 by comparing the propagation of periodic signals and the mean age distribution in models to derivations from observations. We present conclusions in section 6.

2. Models

The models that participated in MM2 encompass several classes of formulation in their approach to simulating the stratosphere. Table 2 summarizes the models that performed the transport components of the suite of MM2 experiments. Included are models having only a latitude-height plane representation of tracer distribution (2-D), as well as fully three-dimensional models (3-D). In general, 2-D models advect tracers by a seasonally and spatially varying residual circulation of stream function ϕ , and diffuse tracers by seasonally and spatially varying diffusion tensors \mathbf{K} designed to mimic the zonally averaged tracer-mixing effects of 3-D wave breaking. However, among these models, there are different approaches for calculating ϕ and \mathbf{K} . In AER, for example, ϕ is determined from heating rate calculations, while \mathbf{K} is independently prescribed. AER thus has a high degree of “tunability” of transport but less physical realism. In other models, \mathbf{K} is derived from theoretical considerations relating it to features of ϕ [Jackman *et al.*, 1988] or from analysis of 3-D model data [Yudin *et al.*, 1999]. Another class of 2-D models are sometimes called “2.5-D” models or “interactive” models, e.g., LLNL, NOCAR, and GSFC-2Dint. These models have a 3-D representation of the propagation of low wave-number planetary waves. Propagation characteristics are determined by the zonal wind field, and the breaking of the waves, in turn, affects the zonal wind.

The residual circulation is computed self-consistently with the zonal wind, and tracers are transported in the zonal-mean plane by the residual circulation and the diffusion due to the wave breaking [Garcia *et al.*, 1992; Garcia and Solomon, 1994].

The 3-D models are all “off-line” chemical transport models (CTMs): they solve the continuity equations of tracers in three-dimensions, given meteorological fields (archived data on wind and convection) from either general circulation models (GCMs) or from assimilations of stratospheric observations. The 3-D models analyzed here are not all independent. For example, MONASH2 and GMI-NCAR employ the same set of GCM data, differing in the numerical advection scheme used by the CTM. GSFC-3D and GMI-DAO employ the same assimilated wind data, differing in the horizontal resolution. MONASH1 and MONASH2 employ related GCM data, with MONASH2 using a version that has stronger gravity wave drag. These CTMs do not simulate inter-annual variability in transport, but instead recycle a single year of meteorological data for multiyear integrations.

3. Age Spectra

3.1. Background

The age spectrum in the stratosphere $G(\mathbf{x}, t|t_0)$ is a type of Green function that propagates a tropospheric mixing ratio boundary condition into the stratosphere, and thus it may be used, for a conserved tracer, to reconstruct the stratospheric response to an arbitrary tropospheric time variation. $G(\mathbf{x}, t|t_0)$ has the interpretation that $G\delta t$ is the mass fraction of air at \mathbf{x} in the stratosphere that was last in the troposphere a time $t - t_0$ to $t - t_0 + \delta t$ ago. The age spectrum was discussed by Kida [1983] and more formally developed by Hall and Plumb [1994]. Here, we briefly focus on several features that have received less attention elsewhere.

$G(\mathbf{x}, t|t_0)$ is determined in a model as the response to the time-dependent boundary condition $\delta(t - t_0)$ spec-

Table 2. Summary of the Models

2-D Models		Type	Reference
1	AER	NI	<i>Ko et al.</i> [1985]
2	CSIRO	NI	<i>Randeniya et al.</i> [1997]; <i>Vohralik et al.</i> [1998]
3	GSFC-2D	NI	<i>Jackman et al.</i> [1996]
4	GSFC-2Dint	I	<i>Rosenfield et al.</i> [1997]
5	HARVARD	I	<i>Jones et al.</i> [1998]
6	LLNL	I	<i>Prather and Remsberg</i> [1993]
7	MGO-UIUC-2D	NI	<i>Zubov et al.</i> [1995]
8	NCAR-2D	I	<i>Park et al.</i> [1999]
9	NOCAR	I	<i>Garcia et al.</i> [1992]
10	SUNY-SPB	NI	<i>Smyshlyayev et al.</i> [1998]
11	UNIVAQ-2D	NI	<i>Pitari et al.</i> [1993]
12	WISCAR	I	<i>Brasseur et al.</i> [1990]; <i>Politowicz and Hitchman</i> [1997]
3-D Models		Circulation	Reference
13	GISS8x10	a	<i>Prather et al.</i> [1987]; <i>Hall and Prather</i> [1995]
14	GMI-DAO	b	A. R. Douglass et al., Choosing meteorological input for the global modeling initiative assessment of high speed aircraft, submitted to <i>Journal of Geophysical Research</i> , 1999, hereinafter referred to as Douglass et al., submitted manuscript, 1999.
15	GMI-GISS	c	Douglass et al., submitted manuscript, 1999
16	GMI-NCAR	d	Douglass et al., submitted manuscript, 1999
17	GSFC-3D	b	<i>Douglass et al.</i> [1996]
18	MONASH1	d	<i>Waugh et al.</i> [1997]; <i>Rasch et al.</i> [1995]
19	MONASH2	d*	<i>Hall and Waugh</i> [1998]
20	UCI21	a	<i>Prather et al.</i> [1987]
21	UCI23	c	<i>Hannegan et al.</i> [1998]
22	UIUC-3D	e	<i>Zubov et al.</i> [1999]
23	UNIVAQ-3D	f	<i>Park et al.</i> [1999]

The acronyms and abbreviations used in the model names are AER, Atmospheric Environmental Research; CSIRO, Commonwealth Scientific Industrial Research Organization; GSFC, Goddard Space Flight Center; HARVARD, Harvard University; LLNL, Lawrence Livermore National Laboratory; MGO, Main Geophysical Observatory; UIUC, University of Illinois at Urbana-Champaign; NCAR, National Center for Atmospheric Research; NOCAR, National Oceanic and Atmospheric Administration and National Center for Atmospheric Research; SUNY, State University of New York; SPB, Saint Petersburg Russian Hydrometeorological University; UNIVAQ, University d'Aquila; WISCAR, University of Wisconsin and National Center for Atmospheric Research; GISS, Goddard Institute for Space Studies; GMI, Global Modeling Initiative; DAO, Data Assimilation Office; MONASH, Monash University; UCI, University of California at Irvine. For 2-D models, "I" indicates interactive models, in which 2-D transport is coupled to 3-D wave propagation. "NI" indicates no coupled wave propagation. For 3-D CTMs, the letters indicate the source of meteorological data: (a) GISS lower resolution GCM [*Rind et al.*, 1988], (b) Goddard Earth Observing System Data Assimilation System (GEOS-DAS) [*Coy and Swinbank*, 1997], (c) GISS higher resolution GCM [*Rind et al.*, 1998], (d) NCAR MACCM2 GCM [*Boville*, 1995], (e) University of Illinois GCM, (f) University d'Aquila GCM.

*NCAR MACCM2 with additional gravity wave sources.

ified over some "forcing region" \mathbf{R} in the troposphere (see Table 1). The delta function in time is approximated by holding \mathbf{R} at a finite value for 1 month, and zero for the duration of the simulation. (Note that the magnitude of the first month value is arbitrary, as G is afterward normalized such that $\int_0^\infty G dt = 1$.) The forcing region varies somewhat from model to model, depending on particular grid spacings. For stratospheric studies the details of \mathbf{R} are unimportant as long as it is within the troposphere, as the troposphere is well-mixed on stratospheric timescales and as nearly all air and tracer enters the stratosphere in the tropics, regardless of tropospheric origin. *Hall and Plumb* [1994]

found in a GCM that moving a near-surface \mathbf{R} from the tropics to midlatitudes to a good approximation introduced only a uniform offset to mean age throughout the stratosphere (about 0.7 year in their model). This insensitivity is further indicated by the near equivalence of mean age as computed from the age spectrum and from simulated SF₆ (shown below), despite the very different distribution of surface boundary condition (see Table 1). In this model study, because our focus is the stratosphere, we consider only the difference between mean age at points in the stratosphere and at the tropical tropopause, thereby removing any small offsets caused by differences in \mathbf{R} from model to model.

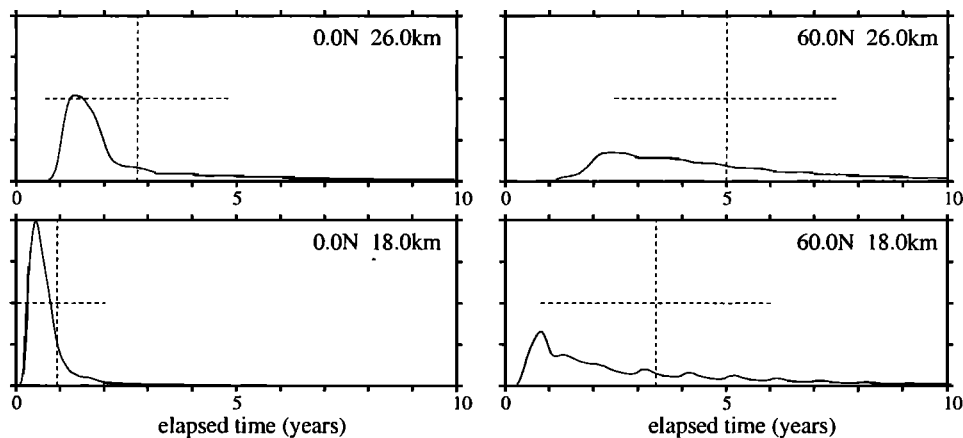


Figure 1. The age spectrum for GSFC-2D at four locations in the latitude-height plane: the equator at 18 km and 26 km, and 60°N at 18 km and 26 km. The mean age is indicated by the vertical dashed line, and the spectral width by the horizontal dashed line.

In general, G is a function of both t and t_0 (or $t - t_0$ and t_0) separately. In this intercomparison, the month corresponding to t_0 is January, and a different start month would yield a different result. Only for stationary transport does G depend exclusively on the elapsed time $t - t_0$. However, as we will illustrate below, seasonality of transport for these models plays only a secondary role in determining many of the annually averaged properties of G . We would get similar results if a different start month had been chosen. Therefore, from here on, we write $G = G(\mathbf{x}, t')$, where $t' = t - t_0$ is the elapsed time, and the separate dependence on t_0 is suppressed. If it were our goal, however, to analyze seasonal variations in G , we would need to perform separate simulations for several source times t_0 throughout the year. For tropospheric studies, the dependence of the age spectrum on \mathbf{R} and t_0 is of comparable importance to \mathbf{x} and $t - t_0$, and a more complete version of G must be considered [Plumb and McConalogue, 1988;

M. Holzer and T. M. Hall, Transit-time and tracer-age distributions in geophysical flows, submitted to *Journal of the Atmospheric Sciences*, 1999].

As an example, we show in Figure 1 $G(\mathbf{x}, t)$ from the GSFC-2D model at the equator and at 60°N and for pressure altitude, z , of 18 km and 26 km. (Note that we use as a vertical coordinate $z = 16 \log(1000/p)$, where p is in hPa and z in kilometers.) See Hall and Waugh [1997a] for MONASH2 and GISS8x10 age spectra at these same altitudes and latitudes. The age spectra are broad, indicating a range of transit times from the troposphere. The spectra tend to be most peaked, and have the shortest transit times, near the tropical tropopause. The first moment, or mean age $\Gamma(\mathbf{x})$, is shown by the vertical dashed line. This quantity can be compared to mean ages derived from observations of temporally-increasing tracers such as CO_2 and SF_6 . For example, to the extent that SF_6 is a conserved tracer whose mixing ratio is increasing linearly in time, its time

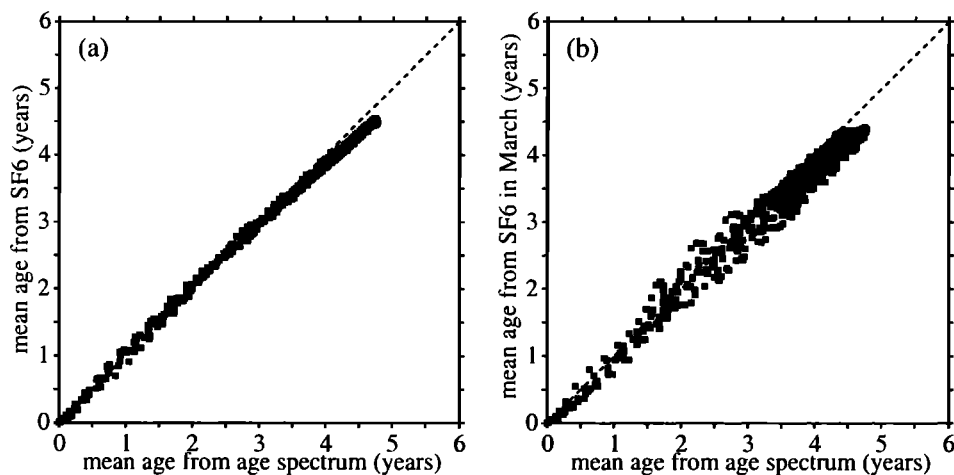


Figure 2. Scatterplots of mean age deduced from the SF_6 simulations (vertical axes) and the age spectrum (horizontal axes) for MONASH2. For Figure 2a the SF_6 age is an annual mean. In Figure 2b the SF_6 lag is for March only. Other models display similar behavior.

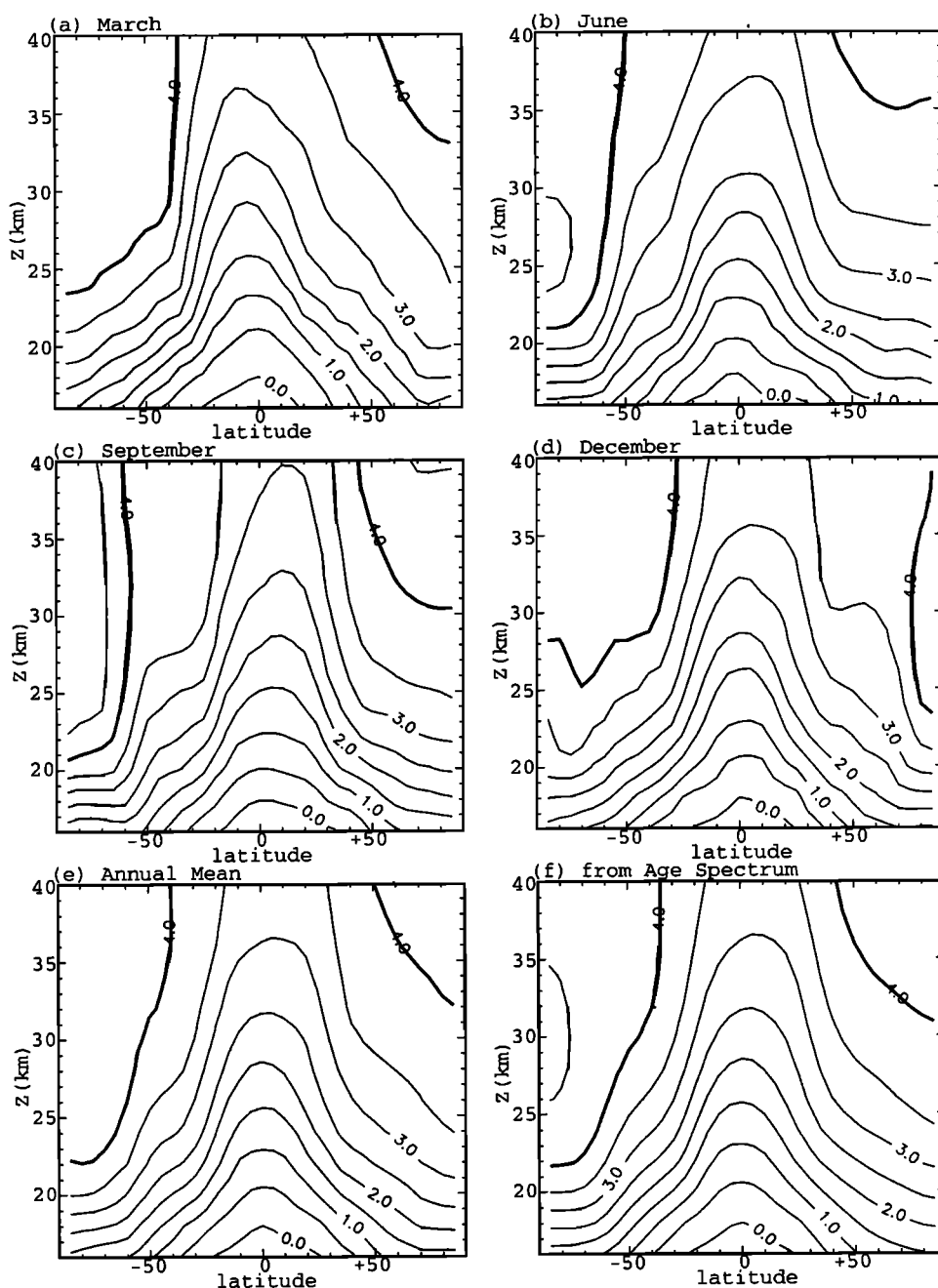


Figure 3. Zonally averaged mean age distribution from MONASH2 for the individual months (a) March, (b) June, (c) September, (d) December, (e) the annual mean, and (f) the age spectral mean, as indicated.

lag at x in the stratosphere from its tropospheric time series is $\Gamma(x)$ [Hall and Plumb, 1994]. Annual cycles of conserved tracers (oscillations of period 1 year, such as those of CO_2 or $\text{H}_2\text{O}+2\text{CH}_4$) in the model stratospheres may also be reconstructed from $G(x, t)$.

3.2. Relation to Other Transport Experiments

As noted above, the formulation of the age spectrum employed here has neglected explicit dependence on time, leaving only dependence on elapsed time from the January source. In the real atmosphere, transport

varies seasonally and interannually, while in these models, transport varies seasonally. Thus, one may ask how faithfully the fields from explicit tracer simulations (e.g., SF_6 and CO_2) can be reconstructed from $G(x, t)$, given the particular January start date.

Figure 2a is a scatterplot for MONASH2 of Γ as derived from the annual mean troposphere-to-stratosphere lag time of a full seasonally varying simulation of SF_6 (see Table 1 for experimental definition) versus Γ as the first moment of $G(x, t)$. The correlation is high. This near equivalence can also be seen in Figures 3e and 3f,

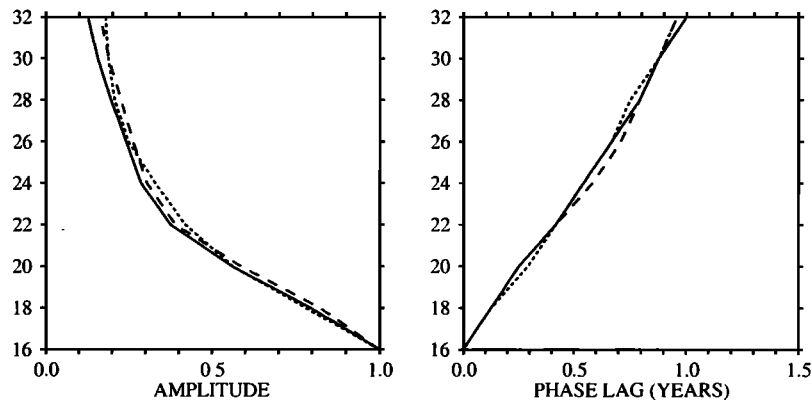


Figure 4. Profiles of the amplitudes $A(z)$ and phase lag times $\tau_w(z)$ of a periodically varying tracer in the AER model as reconstructed from the age spectrum (solid line), from the sin experiment (short-dash line), and from the cos (long-dash line) experiment. Other models display similar behavior.

which show the height-latitude distributions of $\Gamma(\mathbf{x})$ for MONASH2 derived from the two techniques. In Figure 2b, the scatterplot of Figure 2a is repeated, except that the SF_6 lag is for March, rather than an annual mean. The correlation is not as high due to seasonal motions of the mean age isopleths, which cannot be reproduced from the age spectrum for the single value t_0 of January. These isopleth motions can be seen in Figures 3a through 3d, the zonal-mean mean age from MONASH2 for January, April, July, and October. The other models show similar relationships between mean age derived from SF_6 and the age spectrum [Park et al., 1999].

We have also compared the reconstruction of a sinusoid using $G(\mathbf{x}, t)$ with the actual sin and cos runs defined in Table 1. The amplitude $A(\mathbf{x})$ and phase lag time $\tau_w(\mathbf{x})$ from the sin and cos runs and as reconstructed from $G(\mathbf{x}, t)$ are plotted as tropical profiles in Figure 4 for the AER model. Other models display similar behavior [Park et al., 1999]. There are small differences between the reconstructed profiles and those from the explicit sin and cos simulations, as seasonality of transport cannot be reproduced from $G(\mathbf{x}, t)$ for a single t_0 . However, we will show that the differences are smaller than the spread among models and also smaller than the model-observation differences.

We conclude that age spectral reconstructions of the model tracers may be compared to appropriate annual mean observations, even though the age spectra have not been determined as a function of source time t_0 .

4. Global Mean Age

4.1. Observations

There are no global observations of tracers throughout the stratosphere from which mean age can be directly inferred. Thus we do not as yet know the complete mean age distribution in the atmosphere. However, there is a growing body of observations that, taken together, form a picture of mean age in the lower stratosphere and a partial picture in the middle stratosphere.

These pictures have been greatly enhanced by recent high-quality in situ balloon measurements of SF_6 and CO_2 in the tropics and at middle and high latitudes in the lower and middle stratosphere as part of the Observations of the Middle Stratosphere (OMS) campaigns (K. A. Boering et al., manuscript in preparation, 1999; F. L. Moore et al., manuscript in preparation, 1999), which complement previous laboratory measurements of these tracers in whole-air samples collected at middle and high latitudes [Bischof et al., 1985; Schmidt and Khedim, 1991; Harnisch et al., 1996; Patra et al., 1997] and extensive in situ aircraft observations across all latitudes in the lower stratosphere from 1994 to 1997 [Elkns et al., 1996; Boering et al., 1996].

Stratospheric mean age is computed from observations ideally as the lag time in the stratosphere from the tropical tropopause of an inert trace gas with tropospheric sources and steady tropospheric trend. SF_6 and annually averaged CO_2 are two tracers that approximately satisfy the criteria for good mean age estimates. There is good agreement in mean age as inferred from in situ SF_6 and CO_2 measurements made by different experimental groups aboard aircraft [Boering et al., 1996; Elkns et al., 1996] and aboard balloons (K. A. Boering et al., manuscript in preparation, 1999; F. L. Moore et al., manuscript in preparation, 1999). Comparisons among these mean age observations can be seen in Figure 5. (Model's mean ages in the figure are discussed below.) In all panels, symbols with connecting lines indicate observations, with triangles representing in situ CO_2 and diamonds representing in situ SF_6 . Figure 5a illustrates the latitudinal mean age variation at about 20 km. Averages of CO_2 -inferred mean age are computed from in situ aircraft measurements made during 17 time periods from 1992 to 1997 as part of the campaigns Stratospheric Photochemistry Aerosol and Dynamics Experiment (SPADE), Airborne Southern Hemisphere Ocean Experiment/Measurements for Assessing the Effects of Stratospheric Aircraft (ASHOE/MAESA), Stratospher-

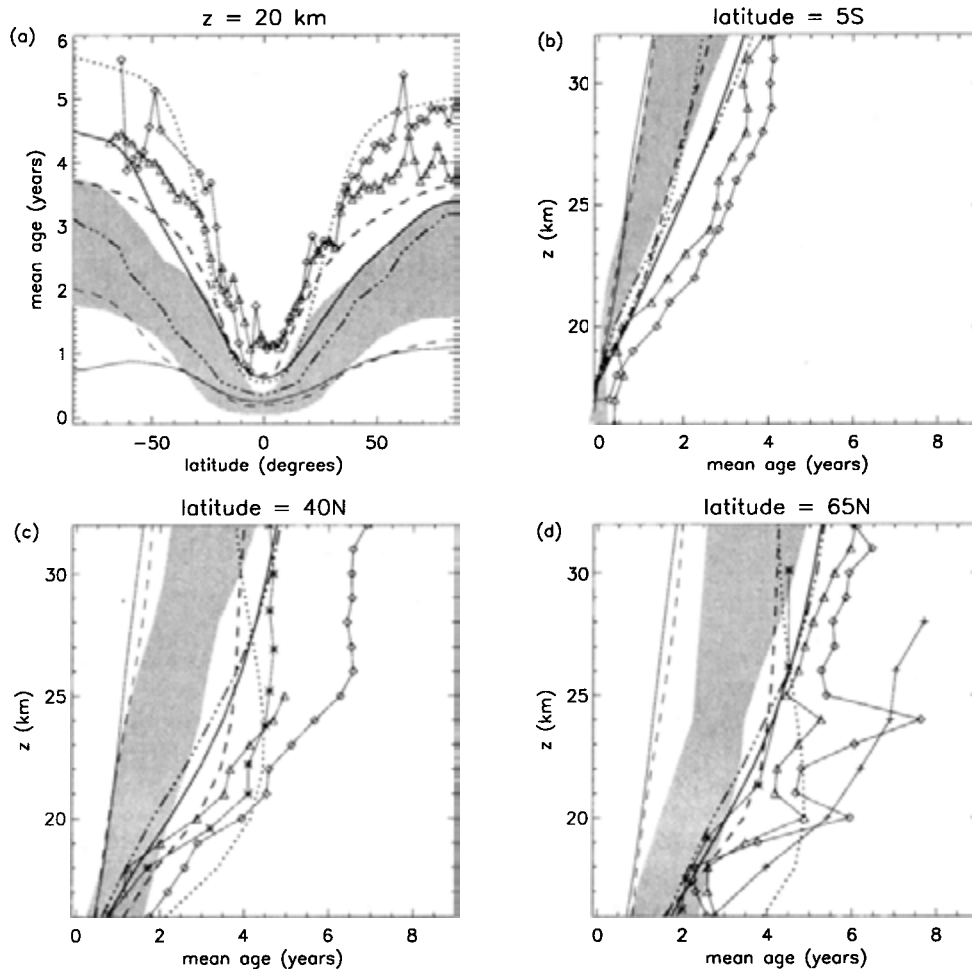


Figure 5. In all panels, the shaded region indicates the range of mean ages of models, with the exceptions of HARVARD (dotted line), MONASH1 (heavy solid line), GSFC-2D (heavy dash line), UCI23 (dot-dash line), GSFC-3D (light dash line), and UIUC (light solid line). The symbols represent observations: mean age from in situ CO_2 (triangles) and in situ SF_6 (diamonds). Observations are as follows: (a) Latitudinal profile of in situ aircraft measurements from SPADÉ, ASHOE/MAESA, STRAT, and POLARIS for CO_2 and from ASHOE/MAESA (one deployment only), STRAT, and POLARIS for SF_6 . Data points are averaged in 2.5° latitude bins (plotted at the midpoint) for both tracers, and in 19.5–21.5 km for CO_2 and 19–21 km for SF_6 . (b) Vertical OMS balloon profiles at 7°N averaged in 1 km altitude bins over three flights for in situ CO_2 (one February, two November 1997) and over two flights for in situ SF_6 (February, November 1997). (c) In situ SF_6 and CO_2 mean ages from a single OMS balloon flight of September 1996, at 35°N , binned in altitude as in Figure 5b, and mean age from SF_6 whole-air samples, September 1993, from 44°N (asterisks) [Harnisch *et al.*, 1996]. (d) In situ CO_2 and SF_6 mean age from the OMS balloon flight of June 1997, 65°N , and whole-air SF_6 samples at 68°N inside (asterisks; average of four flights) and outside (crosses; single flight) the winter polar vortex [Harnisch *et al.*, 1996]. (OMS SF_6 data provided courtesy James W. Elkins and Fred. L. Moore.) See text for further details.

ic Tracers of Atmospheric Transport (STRAT), and Photochemistry of Ozone Loss in the Arctic Regions in Summer (POLARIS); and SF_6 -inferred mean age from the in situ aircraft measurements of ASHOE/MAESA, STRAT, and POLARIS. (Note that the Southern Hemisphere SF_6 data come from a single deployment of ASHOE/MAESA, from October to November, whereas CO_2 was measured during all four deployments, from March to November. A comparison of mean age from SF_6 and CO_2 for just October and November is shown

by Waugh *et al.* [1997].) Data are averaged in 2.5° latitude bins for both tracers, and in 19.5–21.5 km for CO_2 and 19–21 km for SF_6 (data points are centered within the latitude bins). Mean age from SF_6 is computed as done by Volk *et al.* [1997] and provided courtesy of Pavel Romashkin and James W. Elkins. Mean age from CO_2 is calculated as done by Boering *et al.* [1996] as the time lag with respect to the observed CO_2 time series at the tropical tropopause [Andrews *et al.*, 1999]. There is excellent agreement between mean age

from the two tracers equatorward of about 35° , while at higher northern latitudes, SF_6 mean age is 0.4 to 0.8 years older (10% to 20%).

Figure 5b shows vertical profiles of mean age at 7°N from OMS balloon flights. Mean age from in situ CO_2 is averaged in 1 km altitude bins over three flights (one February and two November 1997) and for in situ SF_6 over two flights (February and November 1997). (OMS SF_6 mean age provided courtesy James W. Elkins and Fred L. Moore.) In Figure 5c the in situ SF_6 and CO_2 mean ages are from a single OMS balloon flight of September, 1996, from 35° , binned in altitude as in Figure 5b. Figure 5c also shows mean age from whole-air samples of SF_6 , September 1993, from 44°N (asterisks) [Harnisch et al., 1996]. Finally, in Figure 5d we show profiles at high latitudes: in situ CO_2 and SF_6 of the June 1997, OMS balloon flight from 65°N , and whole-air SF_6 samples at 68°N inside (asterisks) and outside (crosses) the winter polar vortex [Harnisch et al., 1996]. The whole-air profile inside the vortex is an average of data collected over four balloon flights, while the profile outside comes from a single flight.

Agreement in mean age vertical profiles from in situ CO_2 and SF_6 is good in the tropics. At middle and high latitudes, SF_6 -inferred mean age is generally 0.4 to 0.8 years larger than CO_2 , as noted above for the aircraft data. The difference between midlatitude whole-air and in situ measurements seen in Figure 5c is somewhat larger. Harnisch et al. [1996] computed mean age from these whole-air SF_6 samples as the time lag from the northern hemisphere surface mean of Maiss et al. [1996]. For consistency with the other observations and the model results, we have adjusted relative to the tropical tropopause by subtracting 1.4 years (0.6 year to shift from northern surface to global surface [Maiss et al., 1996] and 0.8 from global surface to tropical tropopause [Volk et al., 1997]). This shift, however, is uncertain, due primarily to uncertainty in tropical tropopause SF_6 values. Interannual variability may also play a role in the difference between in situ measurements and whole-air samples, as the profiles come from different years. Other mean age inferences from balloon-borne whole-air samples at midlatitudes fall within the observational range seen in Figure 5c [Bischof et al., 1985; Schmidt and Khedim, 1991], and subtropical profiles [Patra et al., 1997] lie between the profiles shown in Figures 5b and 5c. Finally, OMS in situ CO_2 and SF_6 observations from May 1998 (not shown) yield mean ages similar to the in situ values shown in Figure 5c. At high latitudes, polar vortex air is older than outer vortex air, as indicated by the difference between the high-latitude whole-air profiles in Figure 5d. Note that the in situ mean age from June moves between the inner and outer vortex values, likely evidence for remnants of older vortex air.

There are several sources of uncertainty in mean age inferences from CO_2 and SF_6 . Volk et al. [1997] discussed the relatively small uncertainty introduced upon correcting for the slowly nonlinear tropospheric growth rate of SF_6 . Another possible source of uncertainty is the neglect of mesospheric photochemistry, which may

cause significant errors in mean age inferences at high latitudes in the middle and upper stratosphere [Hall and Waugh, 1998]. In the tropical lower stratosphere, the annual cycle of CO_2 is large enough to complicate mean age inferences [Hall and Prather, 1993; Boering et al., 1994], although its effects can be corrected for [Andrews et al., 1999]. The small source of CO_2 from oxidation of CH_4 introduces some uncertainty [Woodbridge et al., 1995] but is well-accounted for by simultaneous in situ CH_4 measurements [Boering et al., 1996]. Imperfect knowledge of the time history of a tracer at the tropical tropopause introduces uncertainty in the inferred mean age. The extent to which these effects are responsible for the differences seen in Figure 5 between CO_2 - and SF_6 -inferred mean age is unknown and is an interesting and important question that will be addressed in future analyses of observations. Finally, there is uncertainty in the annual and interannual mean age variability in the middle stratosphere that can only be reduced with additional observations. However, as will be discussed below, outside of the polar vortex the observational mean age uncertainty is smaller than the spread among models, and all observations indicate mean ages higher than values simulated by nearly all models. For the purpose of evaluating most of these stratospheric models, agreement among different mean age observations is sufficient.

From the extensive set of measurements, we can make the following general observations about the global Γ distribution, many of which are illustrated in Figure 5. (1) At a given altitude in the lower and middle stratosphere, Γ is smallest in the tropics, i.e., a given Γ contour is higher in the tropics than at midlatitudes. (2) In the subtropics (20°N) and midlatitudes (40°N), above about 24 km, Γ has weak vertical gradient, although it increases rapidly with latitude; i.e., Γ contours are oriented nearly vertically. (3) However, in the subtropics and midlatitudes, below about 24 km, Γ increases rapidly with height. Thus Γ contours which may be oriented nearly vertically aloft, tilt poleward below. (4) At high northern latitudes in summer, Γ increases monotonically with height, at least through 25 km, with the exception of polar vortex remnants. (5) In the lower stratosphere, latitudinal Γ gradients are largest equatorward of about $\pm 30^\circ$. (6) The magnitude of Γ can be 4 or more years (with respect to the tropical tropopause) in the tropics at 30 km and at high latitudes at 20 km.

4.2. Model Measurement Comparison

Figures 6 and 7, which display the mean age distribution for each MM2 model, indicate a wide range of model performance. In the tropics at 40 km, Γ ranges from under 2 years (UIUC-3D, GSFC-2Dint, and models using DAO winds) to over 5 years (UCI23). Although all models show the effects of upwelling in the tropics, producing the characteristic isopleths of long-lived tracers of tropospheric origin, the tropical-extratropical gradients vary widely. Vertical age gradients at high latitudes do not everywhere agree on sign. Some models have age maxima in the high-latitude lower stratosphere, which is not observed, except in

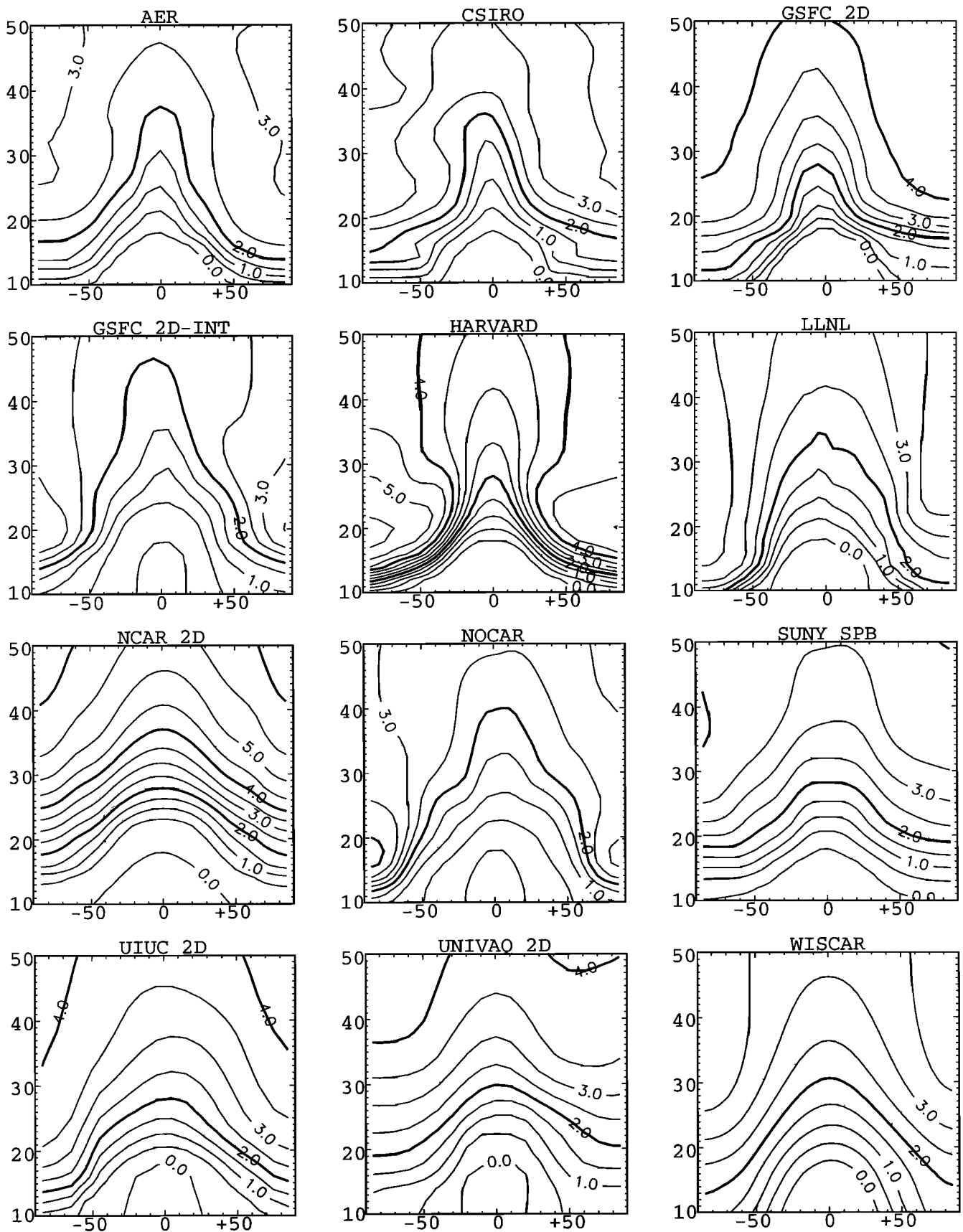


Figure 6. Modeled mean age distributions in the latitude-height plane as derived from the age spectrum. Each panel corresponds to an MM2 two-dimensional model, as labeled. Mean age is taken as zero at the equator and 18 km. Contour intervals are 0.5 year, and the heavy contours indicate 2 year intervals. Negative values are not shown.

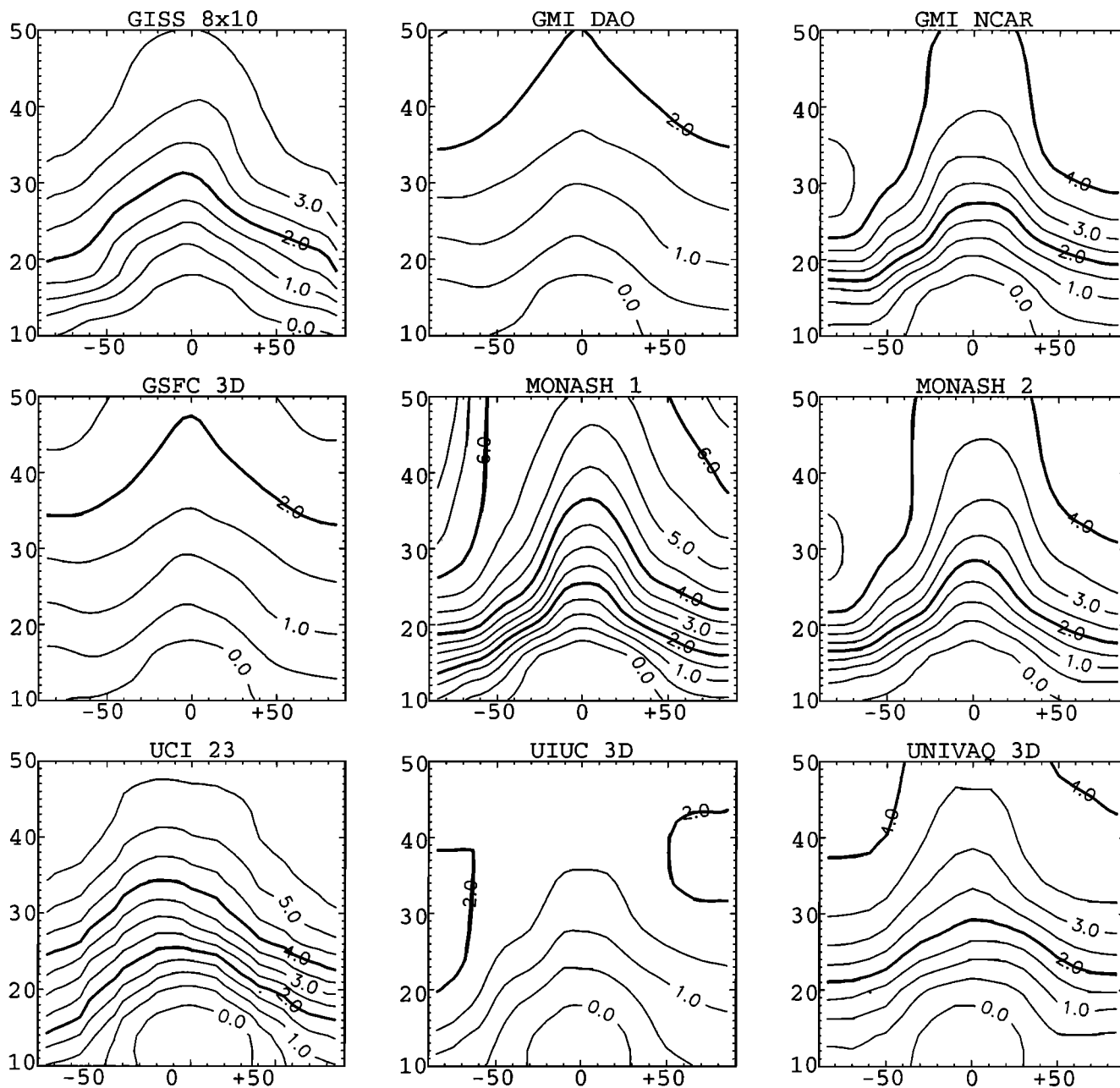


Figure 7. Same as Figure 6, but for three-dimensional models.

thin filaments of vortex air remnants (in situ profiles of Figure 5d). Other models have maxima higher up at high latitudes, or have age increasing monotonically with height throughout the atmosphere.

For direct comparison to observations, the mean ages of the models are plotted in Figure 5. Most models are included in the shaded regions, while several others are plotted individually. The model mean ages are computed from the age spectrum, and are therefore approximately equivalent to annual averages, as discussed in section 3. While the ER-2 aircraft data are extensive, so that the observational means in Figure 5a average over seasonal variations, the vertical profiles of Figures 5b, 5c, and 5d are snapshots in time. How-

ever, except for the high-latitude polar vortex profile, this introduces only a minor inconsistency in the model-observation comparison, as most models display seasonality of mean age small compared to their differences from observations. (See Figures 2 and 3 for MONASH2 seasonality.)

Figure 5 shows that the spread of model mean ages, and the difference of most model mean age values from the observations, is large compared to the observational uncertainty. Most models are significantly too young throughout the stratosphere. The lower stratosphere Γ maximum at middle and high latitudes in several models is a feature not present in observations, with the exception of the polar vortex remnants of late spring

(Figure 5d). Most models do not reproduce the sharp latitudinal gradients in the lower stratosphere observed between 10° and 30° from the equator (Figure 5a).

4.3. Implications for Model Transport

To understand the variation among models, it is useful to categorize them based on the orientation of their Γ contours. Figure 8 shows schematics of three conceptual global Γ orientations. The middle schematic, “class B”, is the most consistent with observed $\Gamma(x)$ features 1 through 5 listed above. In class A, tropical isolation is captured in the large upward bulge of isopleths at low

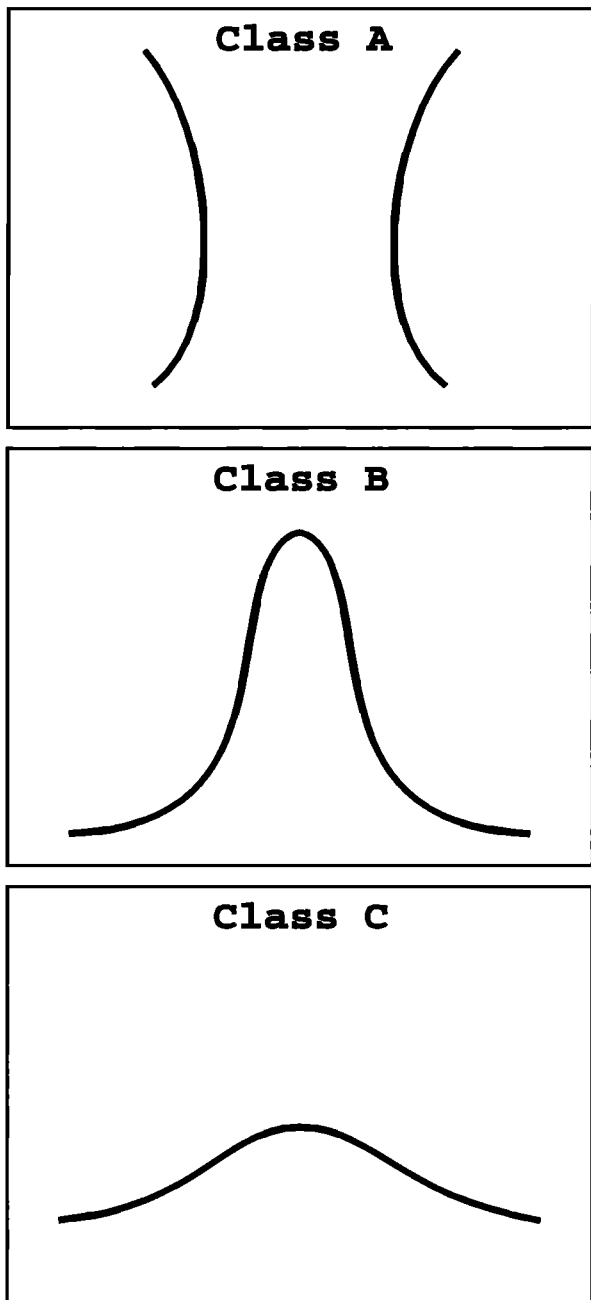


Figure 8. Schematic representation of the variation of the modeled global Γ distribution and its categorization into classes A, B, and C.

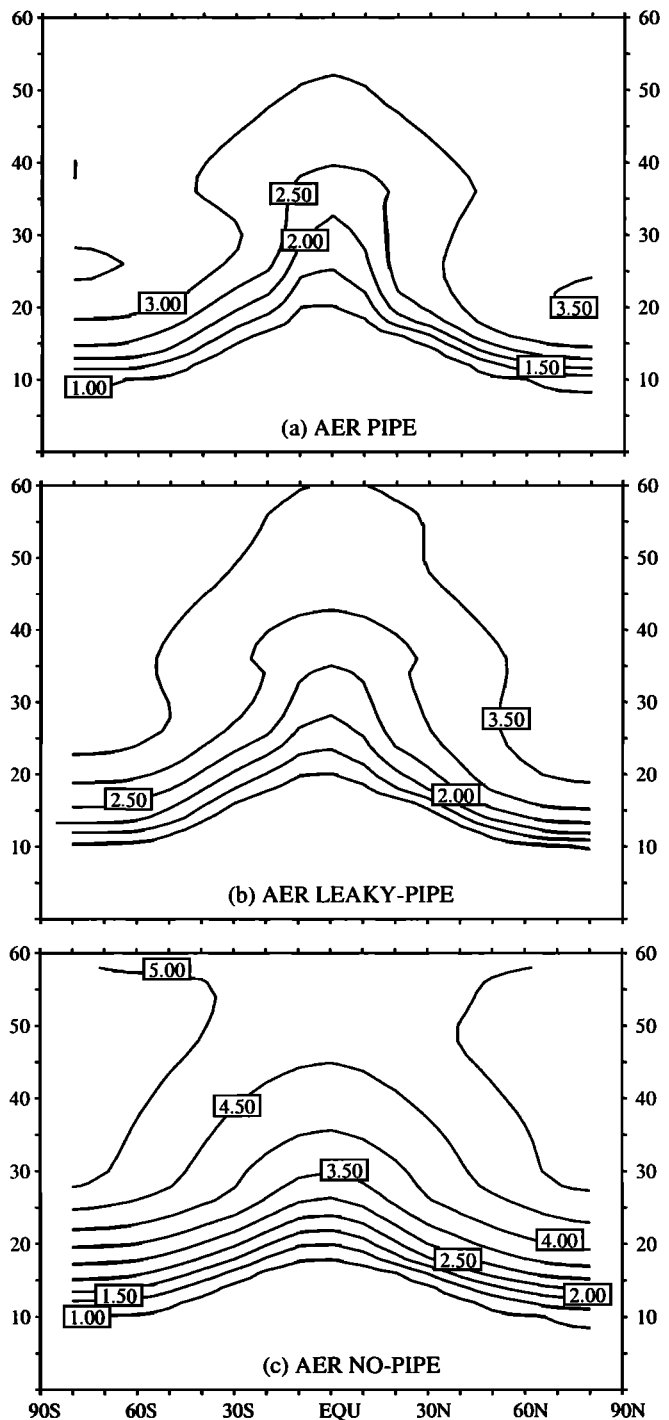


Figure 9. The mean age for (a) the AER “pipe” model, (b) the AER “leaky pipe” model (the version included in MM2), and (c) the AER “no pipe” model (these data courtesy Courtney Scott and Malcolm Ko).

latitudes, but Γ has a lower stratospheric maximum at high latitudes, in disagreement with feature 5. In class C, Γ has no local maxima, but there are also no regions with $d\Gamma/dz$ near zero (weak tropical isolation), in disagreement with feature 2.

We classify the models as follows: Class A: GSFC-2Dint, HARVARD, LLNL, NOCAR; Class B: AER,

CSIRO, GSFC-2D, SUNY-SPB, GMI-NCAR, MONASH1, MONASH2; and Class C: NCAR-2D, MGOUIUC-2D, UNIVAQ-2D, WISCAR, GISS8x10, GMIDAO, GSFC-3D, UCI23, UIUC-3D, UNIVAQ-3D. There is a continuum from class A to B to C, making the classification of models arbitrary in some cases. For example, LLNL could be either A or B, while SUNY-SPB could be B or C. Moreover, other classes could be defined based on different characteristics of the Γ distribution, and models would be grouped differently. In particular, the present classification scheme is determined only by the contour shapes and not by the magnitude of Γ or its gradients, which varies widely among models. Nonetheless, these class definitions suggest variations among models of certain transport mechanisms, which we now discuss.

The presence of relatively flat contours (class C) is consistent with weak isolation of the tropics. If wave activity, parameterized as diffusion in two-dimensional models, reaches too far and too often from the midlatitude "surf-zone" into the tropics, the observed sharp gradients of the mean age (and other long-lived tracers; see below) between the tropics and extratropics will not be realized. For very rapid and uniform mixing, the "global diffuser" limit is reached [Plumb and Ko, 1992; Plumb, 1996]. To illustrate this point, Figure 9 compares three versions of the AER model: the "tropical pipe," the "leaky tropical pipe," and the "no-pipe" models [Shia *et al.*, 1998] (model data courtesy Courtney Scott and Malcolm Ko). In the tropical pipe model, the tropics are isolated by setting latitudinal diffusion (with coefficient K_{yy}) to near zero equatorward of 20° , whereas in the no-pipe model, transport by K_{yy} is significant at all latitudes. The leaky pipe model, the AER version submitted to MM2, is an intermediate case. In the tropical pipe, Γ contours bulge up the most in the tropics, and the extratropical mean age contours slope downward the most steeply.

Mixing of extratropical air into the tropics also increases the mean age throughout the stratosphere by allowing more air to recirculate before exiting the stratosphere. In Figure 9 the no-pipe model has the oldest air overall. Thus increased mixing would seem advantageous, as most MM2 models are too young overall. However, additional extratropical air in the tropics can have the detrimental effects of (1) flattening the Γ contours of models in the extratropics, which may already not be steep enough; and (2) further attenuating the amplitude of the annual cycles in H_2O and CO_2 , which may already be overattenuated, as is discussed in section 5.

Counterintuitively, mixing of extratropical air into the tropics has little effect on latitudinal Γ gradients. For example, while the orientation of Γ contours varies significantly among the three AER models in Figure 9, $d\Gamma/dy$ varies little. Recently, Neu and Plumb [1999] have shown for a simple model that $\Delta\Gamma$ (the difference between extratropical and tropical mean age) is independent of such mixing in the limit of small K_{zz} . This can be appreciated heuristically in the following way: when there is no mixing of extratropical air into the tropics, $\Delta\Gamma$ is given by the transit time around the Brewer-Dobson cell, which is approximated by the residual circulation. If some mixing is added, a fraction δ of tropical air now has extratropical age, increasing Γ overall in the tropics. However, the extratropical mean age increases by an equivalent amount, since the fraction δ recirculates to the extratropics. $\Delta\Gamma$ is unchanged.

Horizontal mixing by K_{yy} diffusion in midlatitudes strongly affects the orientation of mean age contours. Figure 10 shows latitudinal profiles of annual-mean K_{yy} for six 2-D models, averaged from 18 km to 24 km. Although there is wide variation in the magnitudes and gradients, some grouping occurs by model class: Class A models, which are all "interactive" 2-D models, have much smaller midlatitude and high-latitude K_{yy} values

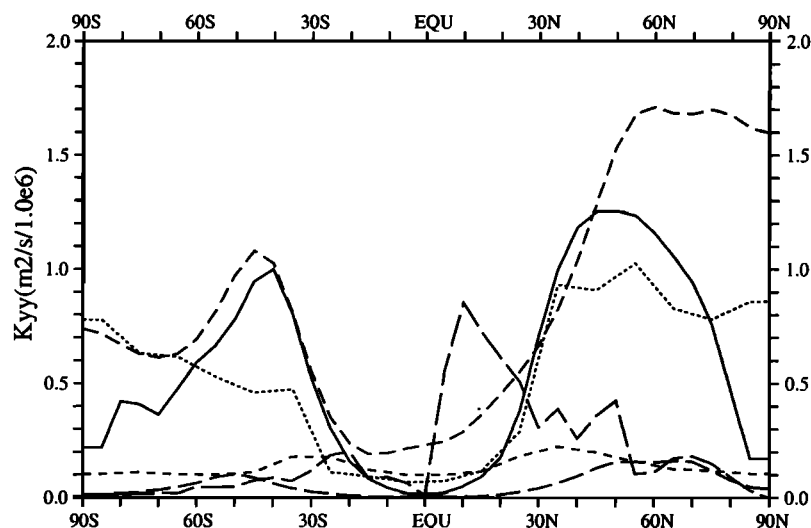


Figure 10. Latitudinal profiles of annual-mean K_{yy} averaged from 18 km to 24 km for five 2-D models: CSIRO (solid line), GSFC-2D (dotted line), GSFC-2Dint (short-dash line), SUNY-SPB (medium-dash line), HARVARD (long-dash line), and LLNL (very-long-dash line).

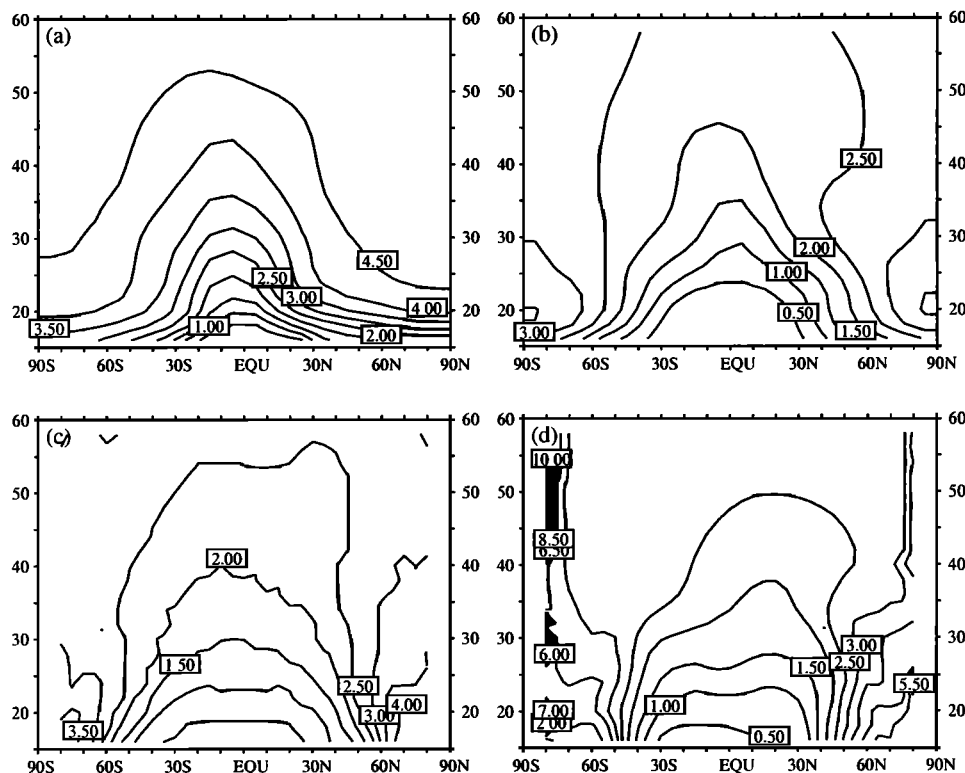


Figure 11. (a) The latitude-height mean age distribution for GSFC-2D. (b) The mean age distribution for GSFC-2Dint. (c) The transit time distribution, using only the GSFC-2D residual circulation for transport. (d) The transit time distribution, using only the residual circulation of GSFC-2Dint for transport.

than other classes, illustrated in Figure 10 by HARVARD, GSFC-2Dint, and LLNL. These low K_{yy} values likely cause the unrealistic high-latitude lower stratospheric age maxima of class A models. Interactive models may be missing important lower stratospheric wave-mixing mechanisms in their formulations.

To illustrate the role of K_{yy} in transport, we compare the mean age distribution to the distribution of transit times obtained from back-trajectories using the residual circulation alone. Figure 11 shows these two quantities for GSFC-2Dint and GSFC-2D. For both models the oldest air from the trajectory calculations is in the high-latitude lower stratosphere, as this represents the longest trajectory along residual circulation streamlines from the tropical tropopause. This distribution is very different from the GSFC-2D mean age, for which horizontal diffusion prevents isolation of old air at high latitudes. Bacmeister *et al.* [1998] and Yudin *et al.* [1999] see similar effects in studies of sensitivity to K_{yy} of their 2-D models. On the other hand, there is little mixing in GSFC-2Dint, the mean age is more similar to the transit time distribution, and the model exhibits a high-latitude lower stratospheric Γ maximum. We note that, in addition to overly weak mixing, unrealistic features in the spatial structure of the residual circulation can also cause a high-latitude lower stratosphere Γ maximum.

The mean age distribution is also strongly affected by the magnitude of the residual circulation. Figure 12 compares the residual circulations and mean age distributions of MONASH1 and MONASH2. These simulations use the same transport model, but wind data from two versions of the NCAR MACCM2 differing in their gravity wave drag. The MACCM2 version whose wind data drives MONASH1 (described by Boville [1995]) employed only orographically forced gravity waves. The northern hemisphere stratospheric climatology was realistic, but the high-latitude southern winter was too cold and the southern polar night jet too strong. To improve the climatology, a revised MACCM2 was run, having additional gravity wave sources. These wind data drive MONASH2. In the revised version, whose southern hemisphere climatology is much improved (although the northern hemisphere is worsened), the additional gravity wave drag causes a more vigorous residual circulation, as seen in Figure 12. Consistent with an increased circulation, the mean age is reduced throughout the stratosphere. Changes in quasi-horizontal mixing due to altered planetary wave breaking, which we have not examined, may also play a role. Contour shapes appear to change only little between the models, and the ratio of MONASH2 to MONASH1 mean age, about 0.8, is fairly uniform through the lower and middle stratosphere. (A detailed comparison of the two

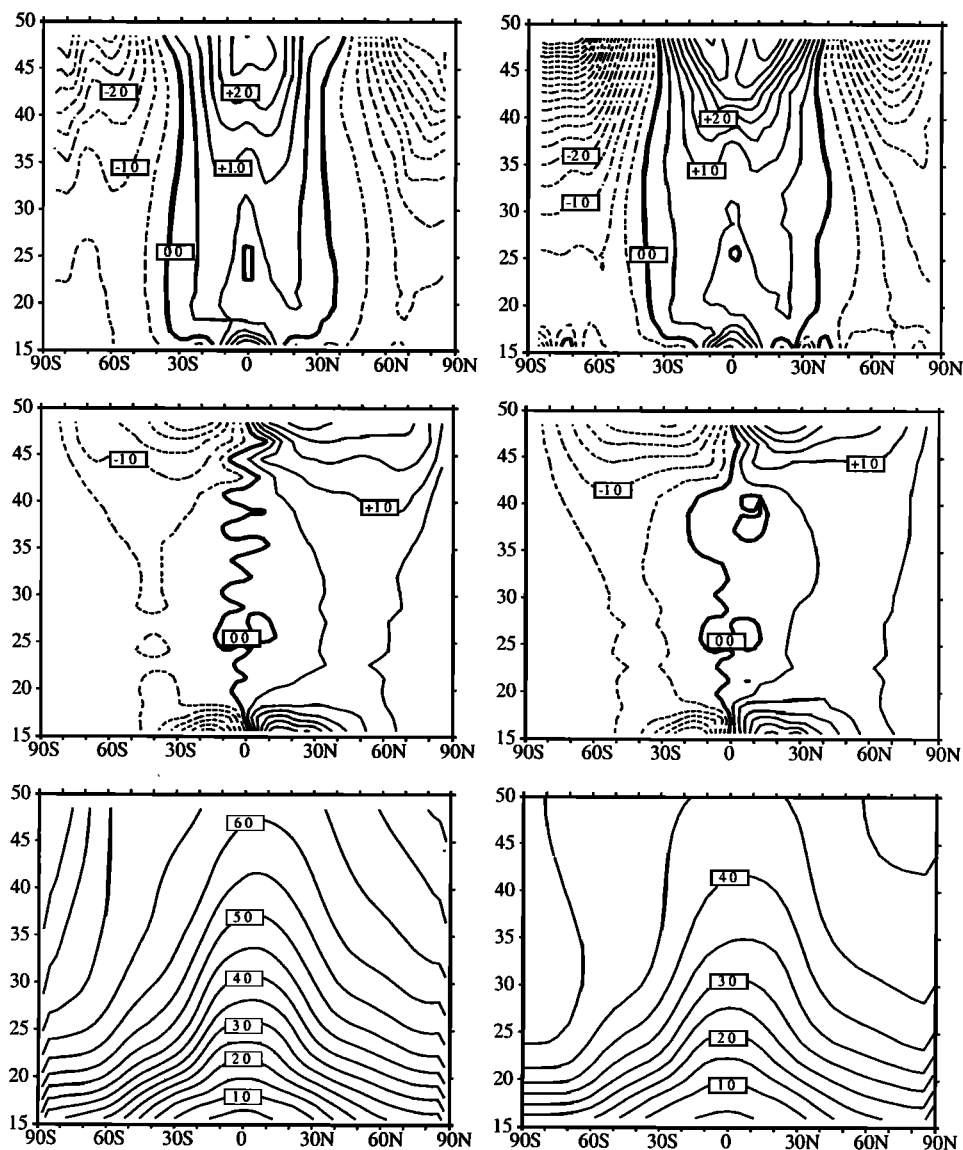


Figure 12. The residual circulation for the two versions of the MACCM2 GCM used by MONASH1 and MONASH2 and the corresponding Γ distributions. The left column is for MONASH1, and the right for MONASH2. The top row is annual mean \bar{w}^* in 0.5 mm/s contours, the middle row is annual mean \bar{v}^* in 0.5 m/s contours, and the bottom row is Γ , in 0.5 year contours. For \bar{w}^* and \bar{v}^* , the dashed contours are negative values, the solid contours are positive values, and the heavy contour represents zero velocity.

MACCM2 versions is currently in preparation.) In their 2-D model, *Bacmeister et al.* [1998] also found that increased mean vertical velocities through the tropical stratosphere (due to larger prescribed tropospheric heating sources in their experiments) resulted in significant mean age reductions.

4.4. Comparison With Other Long-Lived Tracers

The preceding discussion has shown that there is a large variation in the simulated mean ages between models and that the simulated mean ages generally differ greatly from observations. Similar variations can also be seen in simulations of long-lived tracers that are

photochemically active in the stratosphere, although the magnitude of the differences is reduced, particularly for gases of tropospheric origin. Figure 13 shows the annual-mean, zonal-mean N_2O for six models. There is significant variation in N_2O between models, both in isopleth shape and magnitude, albeit the magnitude variation is much less than that of mean age. For example, the isopleths bulge upward sharply in the tropics of HARVARD, while in UCI23, they are relatively flat. The N_2O magnitude at 40 km in the tropics varies from 20 ppb (NCAR-2D) to 100 ppb (GMI-DAO). The observed N_2O from the CLAES instrument on UARS [*Randel et al.*, 1994] is shown at the bottom of Figure 13. Comparison with the simulated fields shows that

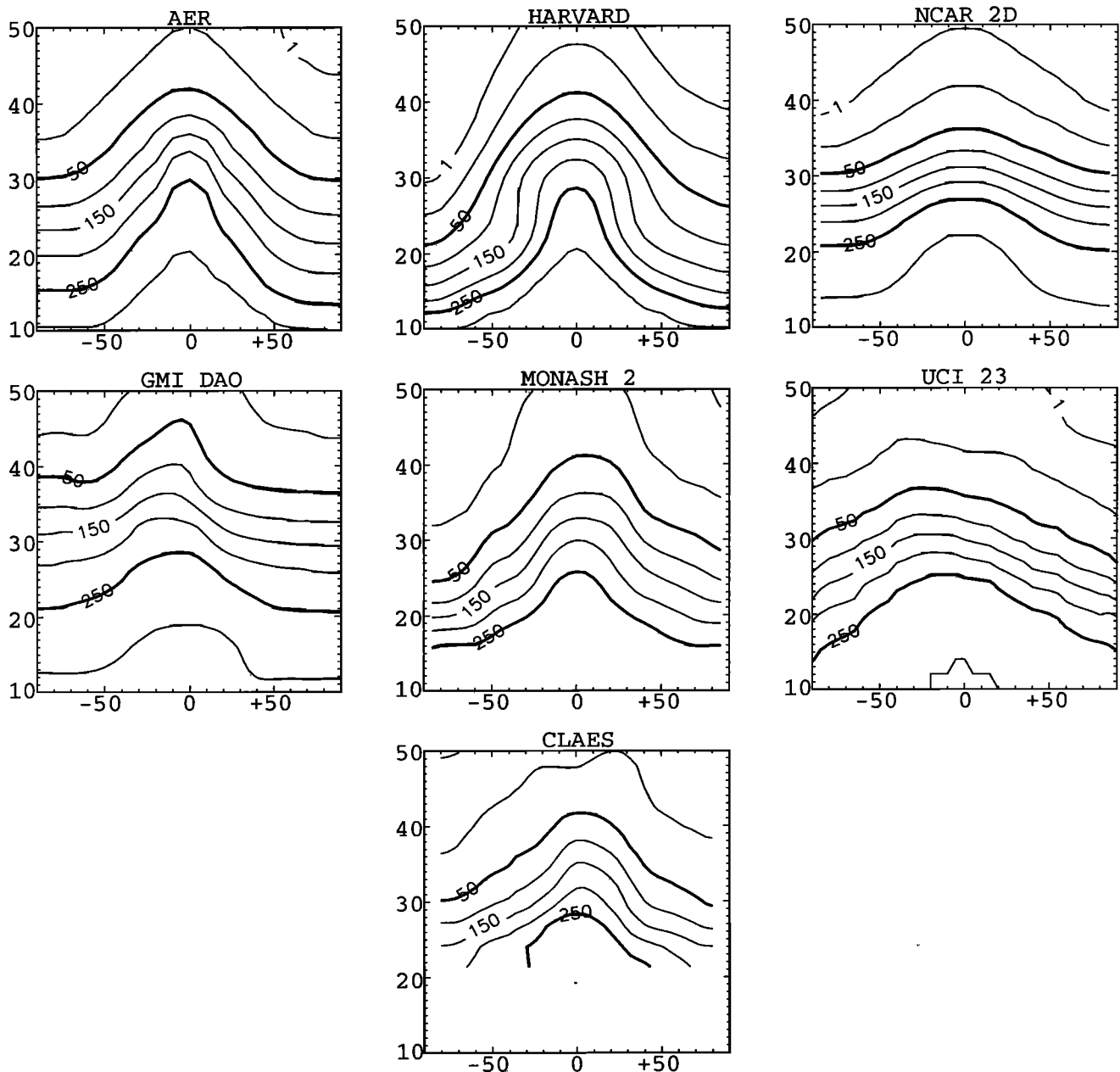


Figure 13. Annual- and zonal-mean N_2O distributions for six MM2 models, as labeled. Contour intervals are 50 ppb, with additional contours shown for 25 ppb and 1 ppb. The N_2O climatology from the CLAES instrument on UARS, adapted from *Randel et al.* [1994], is shown at bottom.

although there is qualitative agreement for most models, there are significant quantitative differences. For example, HARVARD has too little N_2O in the upper stratosphere and the lower high latitude stratosphere, while GMI-DAO has too much in both places.

Comparing the N_2O of Figure 13 to the mean age of Figures 6 and 7 shows that the model-model variation of these two quantities is qualitatively similar. Equatorward of 40° the N_2O and mean age isopleths for a given model are nearly parallel, and models with low mean age generally have high N_2O . At high latitudes, N_2O and mean age isopleth shapes within a model differ more, particularly for class A models (GSFC-2DINT,

HARVARD, LLNL, NOCAR). Because of photochemical loss in the upper stratosphere, N_2O falls off with altitude in all models, whereas the sign of $d\Gamma/dz$ varies among models. Simulations of other long-lived tracers also show consistent model-model differences. For example, Figure 14 compares NO_y and Cl_y for the AER and NCAR-2D models. These families of active chemical species have isopleth shapes qualitatively similar to those of N_2O and Γ : for AER they bulge up sharply in the tropics of the lower and middle stratosphere, while for NCAR-2D they are more flat.

The relationship of the mean age to N_2O , NO_y , and Cl_y is summarized in the lower stratosphere by the scat-

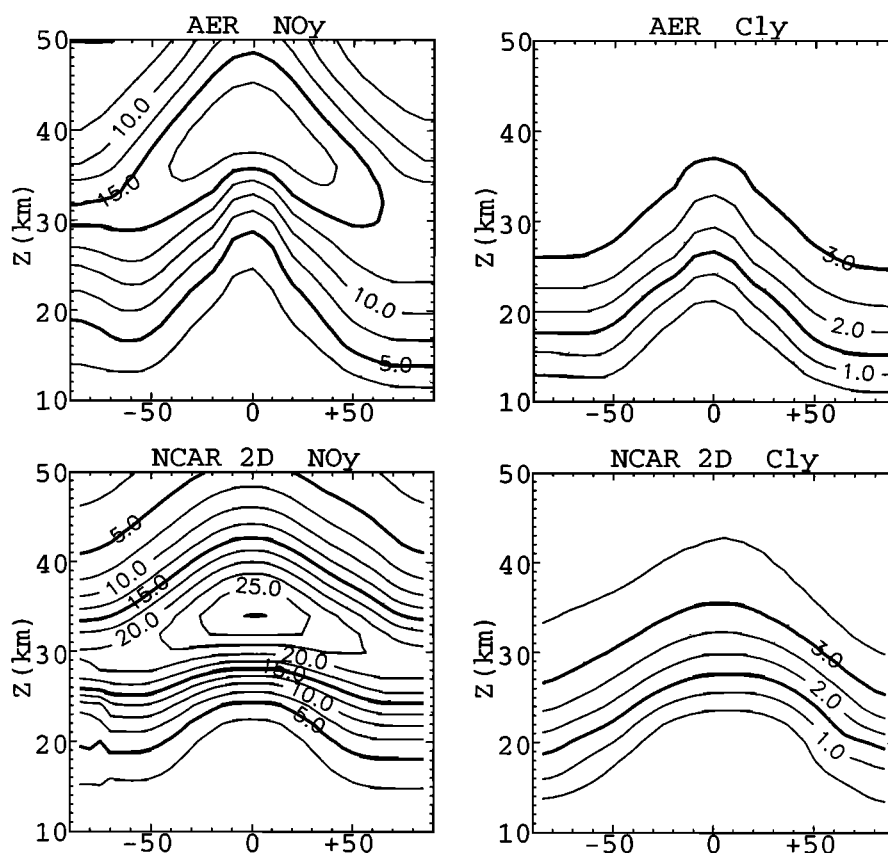


Figure 14. Annual-mean latitude-height distributions of NO_y and Cl_y for the AER and NCAR-2D models, as labeled. These data are from the full chemistry simulations, as defined in the MM2 report [Park et al., 1999]. Contour intervals are 2.5 ppb for NO_y and 0.5 ppb for Cl_y .

terplot of Figure 15, in which the mixing ratios of each of the trace gases are plotted versus Γ at 35°N , 18 km and 55°N , 22 km. Values for nine 2-D models are shown (the models that submitted NO_y and Cl_y data). For all three trace gases there is a good correlation with Γ : the linear correlation coefficient (computed over both locations) is -0.86 for $\Gamma\text{-N}_2\text{O}$, 0.75 for $\Gamma\text{-NO}_y$, and 0.87 for $\Gamma\text{-Cl}_y$. Thus a large fraction of the differences in simulation of each N_2O , NO_y , and Cl_y can be explained by differences in simulation of transport alone. The spread across the nine models in Γ is large, more than a factor of 3 at 35°N , 18 km. For Cl_y the fractional variation across models is comparable at these lower stratospheric points but is smaller aloft (not shown). Model variation in lower stratospheric NO_y is somewhat smaller than that in mean age, and variation in N_2O (about 15% at 35°N , 18 km) is much smaller. We conclude that inaccuracies in model transport, as revealed by the mean age, reflect large uncertainty in modeled Cl_y and NO_y in the lower stratosphere (where these species are under dynamical control) but less uncertainty in the middle and upper stratosphere (where chemical processes becomes more important).

Mean age, N_2O , and Cl_y are correlated because the longer air spends in the stratosphere, the greater its age, the less its N_2O via photolysis, and the greater its Cl_y

via production by CFC photolysis. (NO_y is somewhat more complicated because it has lower stratospheric source and upper stratospheric sink, but the correlation still holds in the lower stratosphere.) However, the correlation with mean age is not perfect. To understand why, consider a lower stratospheric air parcel comprising a small fraction of old air that has spent considerable time at high altitudes. This old air fraction will contribute significantly to the mean age of the parcel, and the older the fraction, the greater its impact on mean age. However, such old air will have lost almost all its N_2O , and thus its N_2O content will be insensitive to its age. Similarly, such old air will have gained nearly all the Cl_y possible (near complete photolytic destruction of CFCs), and thus its Cl_y content will be insensitive to its age. At the other extreme, a fraction of the lower stratospheric parcel that circulates exclusively in the lower stratosphere below the N_2O sink or Cl_y production region will contribute increasingly to the mean age with increasing time spent in the lower stratosphere but will not have lost any N_2O or have gained any Cl_y . Again, the N_2O and Cl_y contents of the fraction are insensitive to its age. In practice, lower stratospheric air comprises a mixture of these two extreme (and intermediate) fractions. While there may be little sensitivity of chemical composition to age variation within

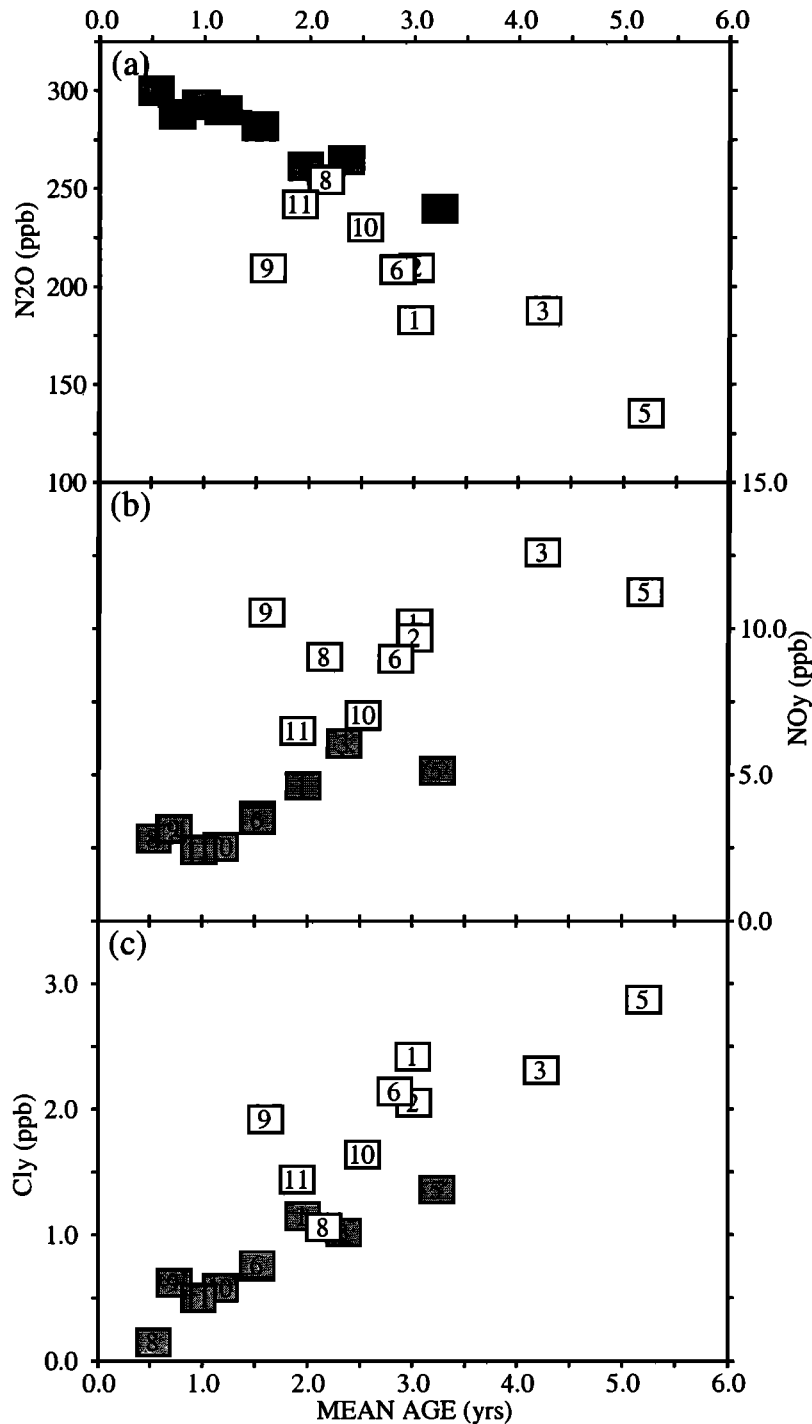


Figure 15. (a) N_2O versus Γ , (b) NO_y versus Γ , and (c) Cl_y versus Γ . The zonally averaged locations represented are $35^\circ N$, 18 km (shaded) and $55^\circ N$, 22 km (unshaded). Numbers in the symbols correspond to models, as listed in Table 2. The values of N_2O , NO_y , and Cl_y are annual means, and Γ is computed from the age spectrum.

each fraction, the chemical composition of the mixture will depend on the relative amounts of young air rich in tropospheric gases and old air rich in photolysis products, thus establishing a correlation, albeit imperfect, between age and chemical composition.

Fractional variations in lower stratospheric Cl_y and NO_y across the models are much greater than varia-

tion in N_2O . Air enters the stratosphere from the troposphere having its maximum stratospheric N_2O mixing ratio, $[N_2O]_0 \approx 310$ ppb, which is the same for all the models. Only a small fraction of $[N_2O]_0$ has yet been destroyed in the lower stratosphere, so that variations from model to model are small compared to the mean across models. On the other hand, new strato-

spheric air has no Cl_y or NO_y , so that variations in the relatively small amount of Cl_y and NO_y in lower stratospheric air are large compared to the means across models. Note that the quantity $[\text{N}_2\text{O}]_0 - \text{N}_2\text{O}$ (not shown) has lower stratospheric model-to-model variation very similar that of Cl_y and NO_y .

5. Tropical Transport

Transport in the tropics of the stratosphere critically affects the distribution of trace gases and the dispersal of aircraft pollutants. Observations of the mean age, $\Gamma(\mathbf{x})$, the amplitude of a propagating annual cycle in mixing ratio, $A(\mathbf{x})$, and the phase lag of the cycle, $\tau_\omega(\mathbf{x})$, represent important constraints on modeled transport in this region.

5.1. Observations

Figure 16a shows tropical profiles of $A(z)$ for models and for inferences from satellite and in situ observations. The heavy solid line is derived from the empirical orthogonal function analysis of Mote *et al.* [1998] of $\dot{H} = \text{H}_2\text{O} + 2\text{CH}_4$ time series from the UARS HALOE instrument's measurements of CH_4 and H_2O from 1992 to 1997 (courtesy Philip Mote). The symbols in the figure are derived from in situ observations of \dot{H} from balloon flights in 1997 and the annual cycle of CO_2 from aircraft and balloon flights from 1994 to 1997 (K. A. Boering *et al.*, manuscript in preparation, 1999).

There is considerable uncertainty in the observational inferences of $A(z)$. While in situ values below about 20 km are in approximate agreement with HALOE, the two values above 21 km are much lower than HALOE. There are several possible reasons for this disagreement. On the one hand, HALOE underestimates significantly the H_2O annual cycle near the tropopause, as can be seen upon comparison of near-tropopause HALOE H_2O measurements to in situ H_2O measurements from aircraft [Mote *et al.*, 1996]. As a result, HALOE overestimates the fractional amplitude aloft. On the other hand, the highest altitude in situ values are derived from very few measurements of \dot{H} and CO_2 in a region shown to be perturbed by filamentary intrusions of midlatitude air [Jost *et al.*, 1998], while the HALOE values come from 5 years of continuous data across the tropics. For this reason, above 20 km we weight more heavily the HALOE data in the subsequent comparisons to model results. We note, however, that different analyses of HALOE \dot{H} yield different A [Mote *et al.*, 1998, Figure 2]. For example, Randel *et al.* [1998] use a different latitude range (4°S to 4°N rather than 14°S to 14°N) and deduce a fractional attenuation of about 0.55 at 21 km compared to 0.45 from Mote *et al.* [1998]. Despite the uncertainties, we will argue below that if one considers amplitude attenuation per vertical wavelength of the annual cycle signal, the observations meaningfully constrain models.

The observed and modeled $\tau_\omega(z)$ are shown in Figure 16b. Here the in situ and remote inferences are in good agreement. For comparison, note that Randel *et al.* [1998], using different HALOE \dot{H} analysis techniques,

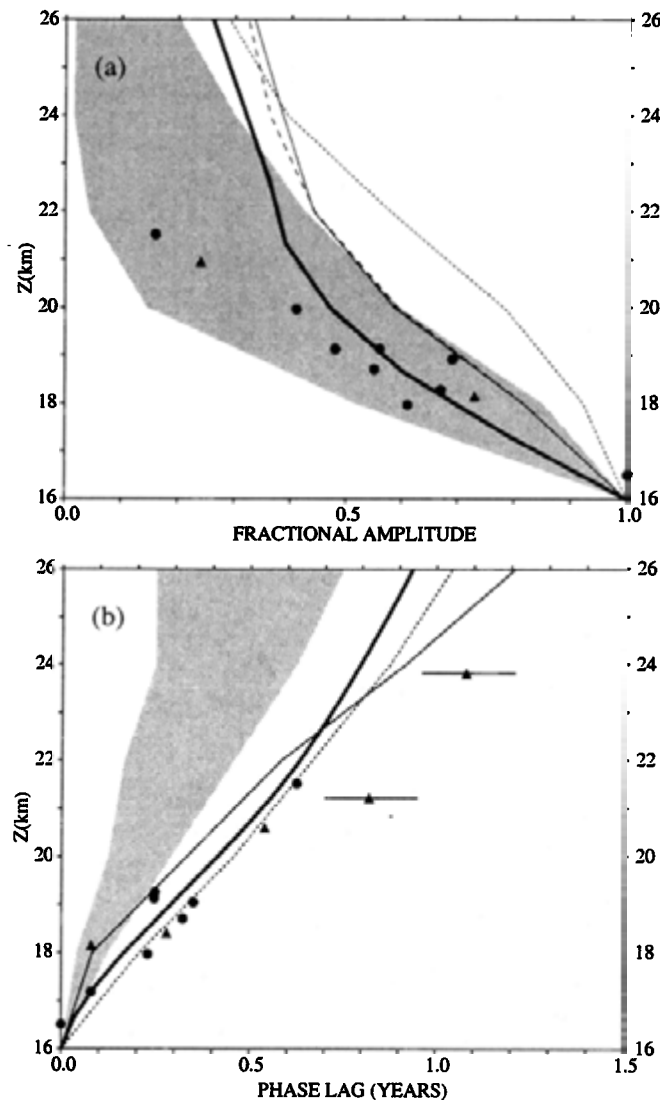


Figure 16. Equatorial profiles of (a) $A(z)$ and (b) $\tau_\omega(z)$ for a range of models and for the observational analyses. All amplitudes are normalized to unity and the phase lag taken as zero at 16 km. The shaded region indicates the range covered by most models, while the individual lines represent several models falling outside the range: (a) GMI-DAO (solid line), GSFC-2Dint (short-dash line), and GSFC-3D (long-dash line); (b), HARVARD (solid line) and GSFC-2D (short-dash line). The heavy solid line represents the analysis of HALOE $\text{H}_2 + 2\text{CH}_4$ [Mote *et al.*, 1998]. The symbols represent analyses of in situ CO_2 (circles) and $\text{H}_2\text{O} + 2\text{CH}_4$ (triangles) measurements (CO_2 from six aircraft and two balloon deployments between 1994 and 1997 and $\text{H}_2\text{O} + 2\text{CH}_4$ from the same 2 balloon deployments in 1997). The error bars on the top two in situ phase lag points are estimated from uncertainty in the tropopause $\text{H}_2\text{O} + 2\text{CH}_4$ time series.

estimate a phase lag of about 0.9 years from 16 km to 24 km, compared to 0.8 years in Figure 16b derived from the Mote *et al.* [1998] analysis. Comparisons of observed and modeled global mean age distributions have been made in the previous section. Tropical profiles are

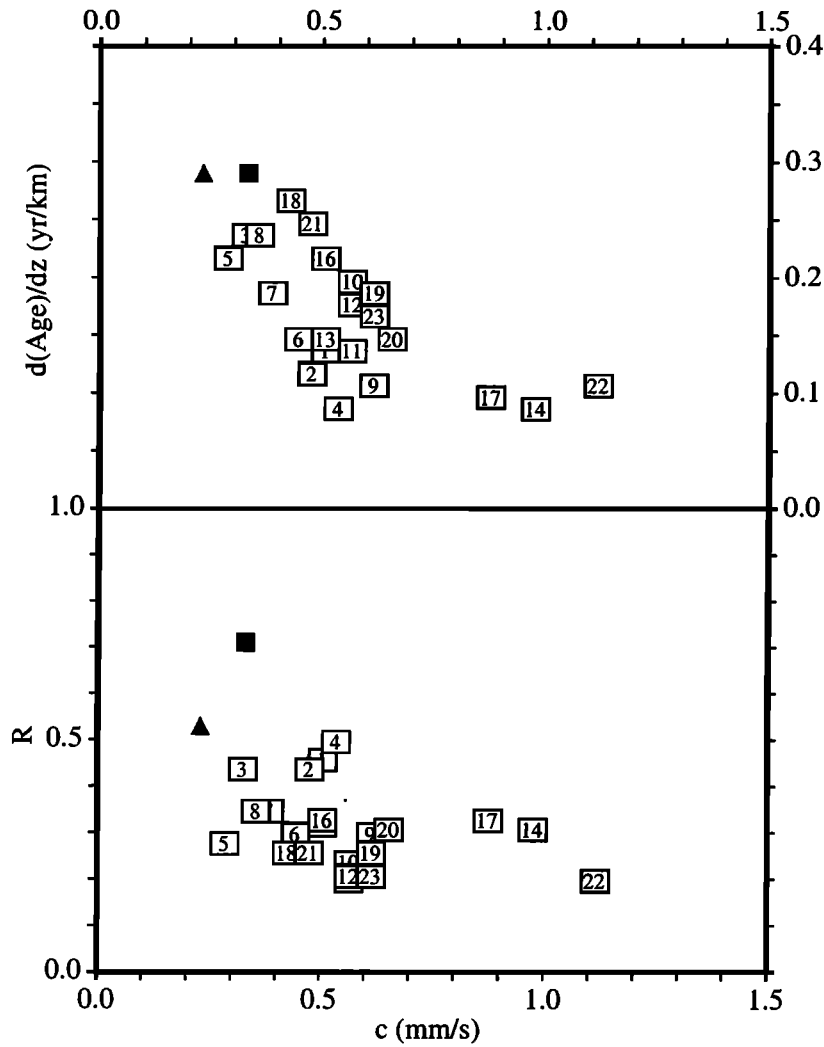


Figure 17. Scatterplots of $d\Gamma/dz$ versus c (top) and R versus c (bottom). Model values are indicated by numbers, as listed in Table 2. The square symbols represent values derived from HALOE $\text{H}_2\text{O}+2\text{CH}_4$ (for R) and in situ SF_6 and CO_2 (for $d\Gamma/dz$), while the triangles represent estimates from in situ CO_2 and $\text{H}_2\text{O}+2\text{CH}_4$ (for R) and CO_2 and SF_6 (for $d\Gamma/dz$).

shown in Figure 5b. Note that $\tau_w < \Gamma$ as predicted by Hall and Waugh [1997a].

5.2. Model-Measurement Comparisons

Figure 16b shows that most models propagate the annual cycle too rapidly in the vertical, while Figure 5b shows that most models significantly underestimate tropical mean age. In Figure 16a, from 16 km to about 20 km the wide range of model performances brackets the HALOE and in situ amplitude, while above about 21 km most models have significantly smaller amplitude than HALOE.

The phase lag time for the models and the measurements to a first approximation increases linearly with height, implying a constant phase speed, c . Using the HALOE τ_w up to 26 km yields $c = 0.33$ ($\Delta z/\Delta\tau_w$ from Figure 16b). For comparison, from the Randel et al. [1998] analysis, $c = 0.28$ mm/s from 16 km to 24 km. When only HALOE τ_w data in Figure 16b to 21 km are used, $c = 0.22$ mm/s is obtained, indicating somewhat

slower upwelling in the lower tropical stratosphere than aloft [Mote et al., 1998]. Fitting a straight line through all the in situ data below 21 km yields $c = 0.23$ mm/s. (Recall that the vertical coordinate is $16 \log(1000/p)$. A more accurate relationship between altitude and pressure results in slightly different values of c .) The phase speeds of the models from 16 km to 26 km range from 0.30 mm/s to 1.09 mm/s (see Park et al. [1999] for individual model values). Most models propagate the annual cycle too rapidly. Note that none of the models has a quasi-biennial oscillation (QBO), which may cause some bias in the time-averaged tropical upwelling (and c) compared to observations. However, the magnitude of QBO variation in tropical upwelling is only about 10% in the lower stratosphere [Randel et al., 1998], small compared to the difference of most of the models' c from the observations. The QBO is not a major factor in evaluation of the models' annual cycle phase speed.

We summarize the mean age variation of the lower

tropical stratosphere (Figure 5b) by its average vertical gradient, $d\Gamma/dz$. The model values of $d\Gamma/dz$ range from 0.26 year/km to 0.08 year/km, all smaller than the value of 0.29 year/km deduced from OMS SF₆ and CO₂. In general, models predict younger air than observed, in some cases by a factor of 2 or more. However, for all models, the phase speed c is larger than $(d\Gamma/dz)^{-1}$, consistent with the observations. (Note that for perfectly isolated tropics with no vertical diffusion, $(d\Gamma/dz)^{-1} = c = w$, the vertical velocity.)

The cycle amplitude of the models and measurements decays exponentially with constant scale height, to a first approximation. From 16 km to 26 km the models attenuate the amplitude with scale heights, H_a , ranging from 2.2 km to 8.7 km (see *Park et al.* [1999] for individual values), while fitting an exponential decay to the *Mote et al.* [1998] HALOE analysis over the same region yields $H_a = 7.6$ km. (For comparison, from the HALOE analysis of *Randel et al.* [1998], a value $H_a \approx 10$ km may be deduced.) The in situ data range up to about 21 km (excluding the highest two points for reasons discussed above) and yield $H_a = 3.8$ km. When only the HALOE points in Figure 16a through 21 km are used, the exponential fit produces $H_a = 5.4$ km, in somewhat better agreement with the in situ observations.

A good measure of the amplitude attenuation is $R = H_a/\lambda$, where $\lambda = c \times (1\text{ year})$ is the vertical wavelength of the annual cycle. What we would most like to infer from $A(z)$ are the rates of processes such as diffusion and entrainment that cause the attenuation of $A(z)$. Normalizing by the wavelength allows each model an equivalent amount of time (1 year) for its attenuating processes to act. Model values of R range from 0.2 to 0.5, compared to 0.7 for the HALOE analyses and 0.5 for the in situ analysis. On a per wavelength basis, most models overattenuate the annual cycle.

Figure 17 displays these model-measurement comparisons graphically. The top panel is a scatterplot of model values of $d\Gamma/dz$ versus c , while the bottom panel shows $R = H_a/\lambda$ versus c . The numbers indicate the models as listed in Table 2, while the symbols indicate the values estimated from satellite and in situ observations. There is some correlation between model values of $d\Gamma/dz$ and c , as both are affected by vertical advection in a model. However, the correlation is not perfect. The quantity $d\Gamma/dz$ is strongly affected by the transport of extratropical air into the upwelling tropical plume, while c is only weakly affected.

5.3. Tropical Transport Mechanisms

As an aid to interpret the differences between model results and the tropical observations in terms of specific transport mechanisms, we use a simple one-dimensional "tropical leaky pipe" (TLP) model of tropical transport

$$\frac{\partial \chi}{\partial t} + w \frac{\partial \chi}{\partial z} - e^{z/H} \frac{\partial}{\partial z} (e^{-z/H} K \frac{\partial \chi}{\partial z}) = -\frac{1}{\tau} (\chi - \chi_e) \quad (1)$$

for a tracer of mixing ratio χ . Here w is a vertical velocity, K a vertical diffusion coefficient, H the air

density scale height, and τ a relaxation time-constant to an extratropical value χ_e , which summarizes the rate at which upwelling tropical air entrains extratropical air. Although real atmospheric and 2-D and 3-D model transport is clearly more complicated, the TLP model is a useful guide.

To illustrate briefly some properties of the TLP model, consider a periodically varying mixing ratio $\cos(\omega t)$ at $z = 0$ (the tropopause). The solution to (1) with constant coefficients, and assuming zero tracer oscillation amplitude in the extratropics, is

$$\chi(z, t) = A(z) \cos[\omega(t - \tau_\omega(z))] \quad (2)$$

where $A(z) = e^{-z/H_a}$, $\tau_\omega(z) = z/c$, and H_a and c are functions of K , w , and τ (see *Hall and Waugh* [1997b] for the explicit expressions). To illustrate the dependencies on the transport coefficients, H_a and c are plotted in Figure 18 versus K and τ for an annual cycle with $w = 0.3$ mm/s. For $K < 0.1$ m²/s, diffusion plays only a small role in the propagation of the annual cycle, and $c \sim w$. At higher K values, diffusion plays a significant role. For all K , the entrainment time τ has little effect on c , as the extratropics adds air with no cycle amplitude, increasing c only to second order. For the amplitude, there are different regimes of dependence on diffusion. For $K < 0.01$ m²/s (and $\tau \leq 2$ years), diffusion plays little role in attenuating the signal. The attenuation is due mostly to dilution by extratropical air, and $H_a \sim w\tau$. For intermediate K (0.01–0.3 m²/s) both diffusion and dilution are important, and for large K (> 0.3 m²/s), diffusion dominates.

Matching TLP solutions (2) to HALOE and ER-2 observations, *Hall and Waugh* [1997b] deduced average values over the lower tropical stratosphere of $w \approx 0.3$ mm/s, $\tau \approx 1.3$ years, and $K \approx 0.01$ m²/s. This roughly agrees with previous independent estimates of τ from 1.0 to 1.5 years [*Minschwaner et al.*, 1996; *Volk et al.*, 1996] and annual averages of estimates of w from heating rate calculations [*Rosenlof*, 1995; *Eluszkiewicz et al.*, 1996]. *Mote et al.* [1998] matched a TLP model with height varying coefficients to HALOE data, deducing K the same order as *Hall and Waugh* [1997b]. *Mote et al.* [1998] deduced a sharp local maximum in τ around 22 km, but averaged from 16 km to 26 km, their $\tau \approx 1.6$ years.

These estimates for K , τ , and w are in the low diffusion regime of Figure 18. Over the tropical lower stratosphere entrainment of extratropical air appears to be the primary attenuation mechanism and advection the primary propagation mechanism of the annual cycles in H and CO₂. Given the models' large deviations from the observations, averaged transport coefficients from observations are most appropriate for comparison. Ultimately, however, if detailed comparisons to observational inferences are to be made, the disagreements among the various observational inferences must be resolved.

Figure 19 illustrates the relative roles that vertical diffusion and advection play in transporting the annual cycles in four 2-D MM2 models. The quantities plotted

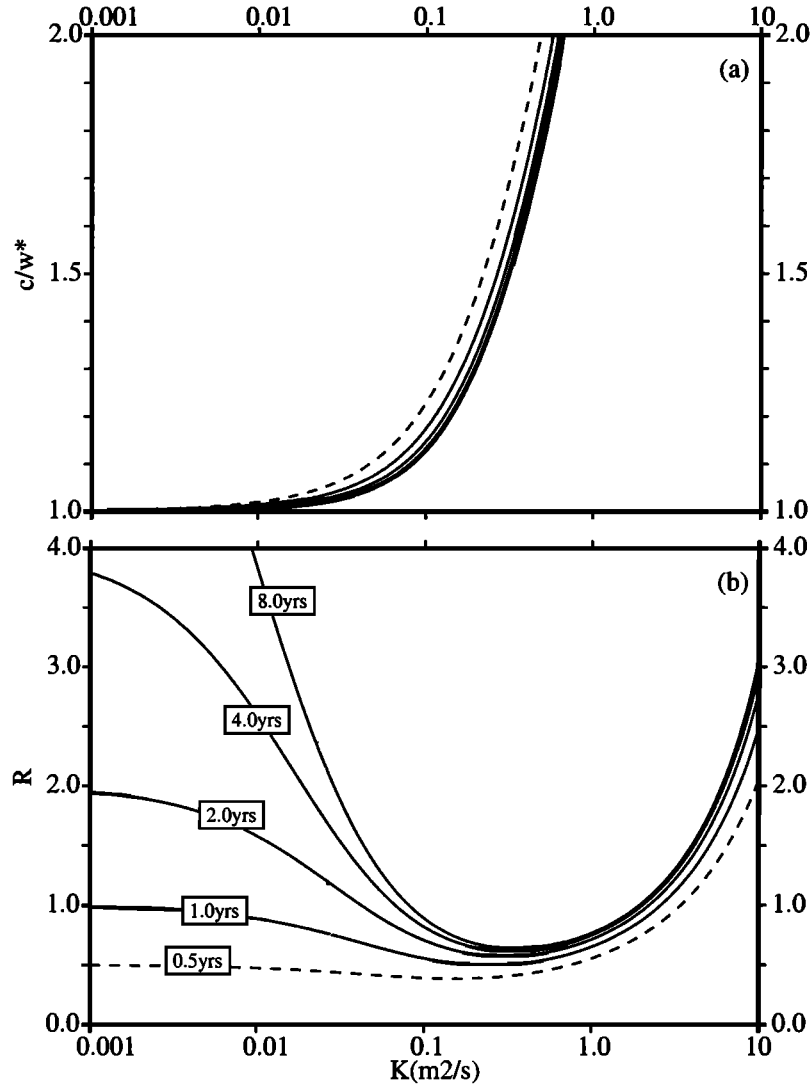


Figure 18. The dependence of (a) c/\bar{w}^* and (b) R on K in the simple tropical leaky pipe model for $\tau = 0.5, 1.0, 2.0, 4.0,$ and 8.0 years ($\tau=0.5$ years is indicated by a long-dash line). For these curves, $\bar{w} = 0.3$ mm/s.

are (1) annually averaged K_{zz} , the vertical component of the model’s diffusivity tensor (interpreted as K in the context of the TLP model); (2) annually averaged model τ_w , whose slope is c ; (3) τ_w from the HALOE \hat{H} analysis; and (4) the timescale for advection by the models’ vertical residual circulation \bar{w}^* . For GSFC-2D (Figure 19a), $K_{zz} < 0.1$ m^2/s throughout the tropical stratosphere, putting it in the low diffusion regime of the TLP model (Figure 18a), so that $c \approx \bar{w}^*$. Moreover, the upwelling rate agrees fairly well with HALOE \hat{H} analyses. For GSFC-2Dint (Figure 19b) $K_{zz} \gg 0.1$ m^2/s below 22 km. As a consequence, the τ_w profile is significantly steeper than the advective time (i.e., $c > \bar{w}^*$). In this regime, diffusion plays a large role in transporting the signal (Figure 18a), contrary to the estimates from observations. CSIRO (Figure 19c) is an intermediate case. The advective time is close to the phase lag from HALOE, suggesting a realistic \bar{w}^* .

However, $K_{zz} > 0.1$ m^2/s , and $c > \bar{w}^*$. SUNY-SPB (Figure 19d) has $K_{zz} \approx 0.5$ m^2/s , which again results in $c > \bar{w}^*$. (More typical implementations of the SUNY-SPB model use much smaller K_{zz} , as discussed by Yudin *et al.* [1999].)

From this analysis, we conclude that several 2-D models have explicit values of K_{zz} that are too large, in some cases by more than an order of magnitude. The 3-D models, on the other hand, have no explicit vertical diffusion. A few 3-D models (UCI23, GMI-NCAR, MONASH1) have values of c that are not too far from that observed (see Figure 17), while others propagate the signal too quickly (GMI-DAO, GSFC-3D, MONASH2, UNIVAQ-3D, GISS8x10). A large value of c could be due to an overly vigorous residual circulation, too much diffusion associated with resolved features of the flow, or too much diffusion implicit in the numerical advection scheme. Numerical diffusion

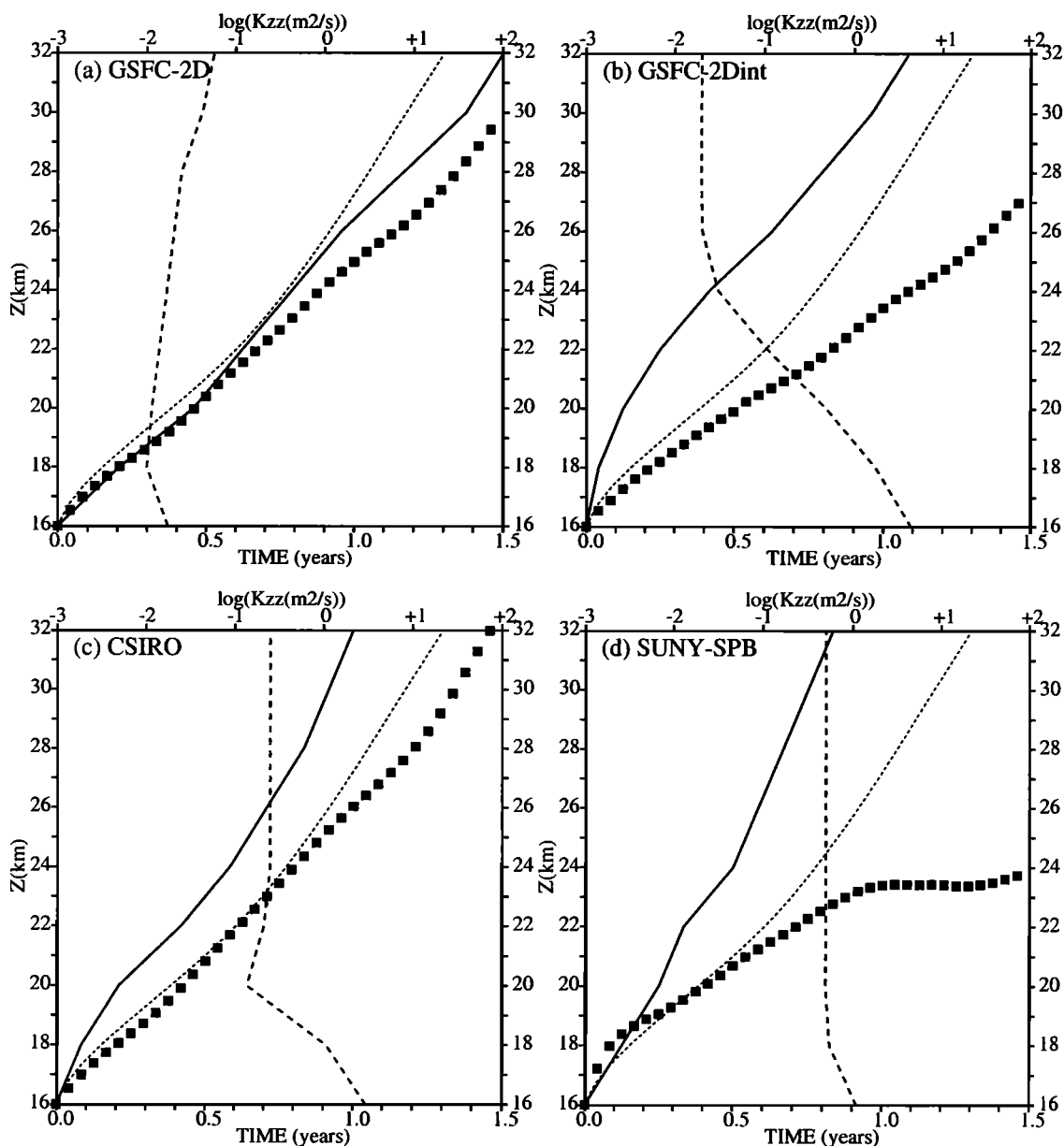


Figure 19. Tropical profiles of model annually averaged K_{zz} (top log scale; dashed line), model τ_w (bottom scale; solid line), HALOE $\text{H}_2\text{O}+2\text{CH}_4$ τ_w (bottom scale; dotted line), and model advective time by \bar{w}^* (bottom scale; symbols). The different panels correspond to different models: (a) GSFC-2D, (b) GSFC-2Dint, (c) CSIRO, and (d) SUNY-SPB.

depends on the particular advection scheme and resolution employed by the model. We have not systematically tested the schemes employed by MM2 models, a study which would be valuable. However, one-dimensional tests show that the second-order moments scheme [Prather, 1986], at least, does not significantly attenuate a sinusoid with as few as four grid points per wavelength. Thus, for example, numerical diffusion should not be an issue for UCI23.

6. Conclusions and Discussion

In this paper we have reported on simulations from a large set of stratospheric models of the mean age and

propagating cycles due to periodic variations of conserved tracers at the tropopause. These simulations have been compared to recent observations in the lower and middle stratosphere. Three general conclusions may be drawn. (1) There is large variation in transport among models, producing mean age fields that vary by more than a factor 2. There is no significant grouping by dimensionality (2-D versus 3-D). (2) Most models have mean ages throughout the stratosphere that are significantly lower than observations, in some models and locations by a factor greater than 2. (3) Model-to-model variation in N_2O , NO_y , and Cl_y in the lower stratosphere is well correlated with variations in mean age, indicating that uncertainty in simulation of these

species in the lower stratosphere (as defined by the spread across model results) is due, in large part, to uncertainty in model transport. The fractional magnitude of model-to-model variation in N_2O is much less than mean age, but for NO_y and Cl_y it is comparable to mean age. We conclude that inaccuracies in model transport have significant impact on simulations of the chemical state of the lower stratosphere.

In addition, we draw several more specific conclusions and isolate some aspects of model transport that need improving. (4) Several models (AER, CSIRO, GSFC-2D, SUNY-SPB, GMI-NCAR, MONASH1, MONASH2) have realistic zonally averaged contour shapes of mean age ("class B" in the nomenclature of section 5), but except for MONASH1, the magnitude of their mean ages is still too small. Other models have unrealistic features in their contour shapes ("class A" or "class C" depending on features) in addition to low mean ages. (5) Several two-dimensional models have explicit vertical diffusion that is too large (i.e., their values of K_{zz} are too large). (6) Models that compute planetary wave propagation and breaking interactively with the circulation tend to have local maxima in the high-latitude lower stratosphere, which is not observed. This suggests that quasi-horizontal mixing is too weak (i.e., values of K_{yy} are too small). (7) The vertical phase velocity in the tropics of a tracer with an annual cycle such as H_2O+2CH_4 and CO_2 is too rapid in most models. This fact, combined with low mean ages, indicates that vertical upwelling in the tropics is too rapid, although in certain 2-D models a significant part of the phase velocity is due to their large vertical diffusion. (8) Many models have tropics that are not isolated enough from midlatitudes, as evidenced by the overattenuation per wavelength of an annual cycle tracer and in the unrealistically "flat" mean age contours (class C models). For some models, vertical diffusion within the tropics may be responsible for the overattenuation.

We have not systematically examined the impact on long-lived tracer transport of numerical aspects of model formulation such as advection algorithm, grid resolution, and coordinate system. Such a study would be worthwhile, as all model formulations result in some degree of tracer diffusion, which in effect, represents transport due to unresolved motions. Nonetheless, some conclusions can be drawn with regard to certain models. The mean age distributions are similar for the 3-D models MONASH2 and GMI-NCAR, which differ only in their advection algorithm ("semi-Lagrangian" [Rasch, 1994] for MONASH2 and "flux-form semi-Lagrangian" [Lin and Rood, 1996] for GMI-NCAR). On the other hand, models having the same advection algorithm, resolution, and other aspects of numerical formulation, but differing in their large-scale circulation (e.g., MONASH1 and MONASH2), have significant mean age differences. This suggests that for at least some of the models the choice of advection algorithm plays only a minor role in determining mean age, compared to the major role played by large-scale features of the circulation such as the residual circulation and quasi-horizontal wave mixing (explicit in 3-D; parameterized diffusively in 2-D).

It is important to appreciate that many components of transport, such as advection by the residual circulation and mixing of extratropical air into the tropics, are highly coupled. The coupling is dynamical for models that compute the circulation in a self-consistent way. However, even for models that prescribe the components explicitly, their effects on tracers are coupled. For example, we have seen that slowing the residual circulation and enhancing the mixing of extratropical air into the tropics both increase mean age. Although increasing mean age is clearly desirable in models in light of the observations, changing either of these transport components independently (which may not even be possible in dynamically self-consistent models) could have detrimental effects on the shape of mean age contours. A tropical region that is uniformly less isolated in the lower and middle stratosphere would, for most MM2 models, cause the shape of mean age contours to be "flatter" in the extratropics and thus more unrealistic than they already are. A less vigorous residual circulation might have a similar contour flattening effect, as mixing processes are provided more time to entrain extratropical air into the tropics.

Despite these couplings, the magnitude of tropical upwelling likely provides the most leverage on the mean age. In the 2-D model study of *Bacmeister et al.* [1998], values of mean age through the tropical stratosphere varied in roughly inverse proportion to the upwelling rate in the 16 km to 20 km region (which, in turn, was varied by changing parameterized tropospheric heating rates), while the slopes of the mean age contours in the extratropics were less strongly affected. Varying planetary wave forcing had less effect on tropical upwelling or mean age but more on contour shapes. Potential complications arise, however, from other constraints on models imposed by photochemically active trace gases. For example, reducing upwelling rates may increase the stratospheric lifetimes of CFC-11 and CFC-12, which for many MM2 models are already too large [Park *et al.*, 1999] compared to the observationally based estimates of *Volk et al.* [1997]. There is, however, large uncertainty in the lifetime estimates.

Mean age highlights the limits of our ability to model global stratospheric transport. Most of the models in MM2 are found wanting in several respects, when compared to observations. The path toward more realistic simulation of transport is not obvious, but it seems clear that continuing sensitivity studies to various aspects of model formulation in two and three-dimensions are necessary.

Acknowledgments. We thank all the participants in the Models and Measurements II intercomparison for their effort and model data. Curtis Rinsland contributed significantly to analysis of model SF_6 data and comparison to observations. Philip Mote provided his HALOE analyses, James W. Elkins and Pavel Romashkin provided SF_6 ER-2 data, James W. Elkins and Fred L. Moore provided recent OMS balloon SF_6 data, Jochen Harnisch provided balloon SF_6 data, and Arlyn Andrews provided binned ER-2 CO_2 data. We acknowledge the many people responsible for the aircraft campaigns SPADE, ASHOE/MAESA, STRAT, and

POLARIS without which these and other model evaluations would not be possible. These missions are funded by the National Aeronautics and Space Administration (NASA). We thank Malcolm Ko and Courtney Scott for additional AER model data. We also thank James W. Elkins, Charley Jackman, Malcolm Ko, Don Wuebbles, David Rind, Doug Rotman, and Hans Schneider for many discussions on issues raised in this work; Will Heres for assistance with model data analysis; and Karen Sage and Jae Park for logistical support in the MM2 intercomparison. Comments from three anonymous reviewers led to an improved manuscript. This work is supported by the NASA Atmospheric Chemical Modeling and Analysis Program and Atmospheric Effects of Aviation Program.

References

- Andrews, A. E., K. A. Boering, B. C. Daube, and S. C. Wofsy, Empirical age spectra from observations of stratospheric CO₂: Mean ages, vertical ascent rates, and dispersion in the lower tropical stratosphere, *J. Geophys. Res.*, in press, 1999.
- Bacmeister, J. T., D. E. Siskind, M. E. Summers, and S. D. Eckermann, Age of air in a zonally averaged two-dimensional model, *J. Geophys. Res.*, **103**, 11,263–11,288, 1998.
- Bischof, W., R. Borchers, P. Fabian, and B. C. Kruger, Increased concentration and vertical distribution of carbon dioxide in the stratosphere, *Nature*, **316**, 708–710, 1985.
- Boering, K. A., B. C. Daube, S. C. Wofsey, M. Loewenstein, J. R. Podolske, and E. R. Keim, Tracer-tracer relationships and lower stratospheric dynamics: CO₂ and N₂O correlations during SPADE, *Geophys. Res. Lett.*, **21**, 2567–2570, 1994.
- Boering, K. A., S. C. Wofsy, B. C. Daube, H. R. Schneider, M. Loewenstein, and J. R. Podolske, Stratospheric mean ages and transport rates derived from observations of CO₂ and N₂O, *Science*, **274**, 1340–1343, 1996.
- Boville, B. A., Middle atmosphere version of the CCM2 (MACCM2): Annual cycle and interannual variability, *J. Geophys. Res.*, **100**, 9017–9039, 1995.
- Brasseur, G., M. H. Hitchman, S. Walters, M. Dymek, E. Falise, and M. Pirre, An interactive chemical dynamical radiative two-dimensional model of the middle atmosphere, *J. Geophys. Res.*, **95**, 5639–5656, 1990.
- Coy, L., and R. Swinbank, Characteristics of stratospheric winds and temperatures produced by data assimilation, *J. Geophys. Res.*, **102**, 25,763–25,781, 1997.
- Douglass, A. R., C. J. Weaver, R. B. Rood, and L. C. Coy, A three-dimensional simulation of the ozone annual cycle using winds from a data assimilation system, *J. Geophys. Res.*, **101**, 1463–1474, 1996.
- Elkins, J. W., et al., Airborne gas chromatograph for in situ measurements of long-lived species in the upper troposphere and lower stratosphere, *Geophys. Res. Lett.*, **23**, 347–350, 1996.
- Eluszkiewicz, J., et al., Residual circulation in the stratosphere and lower mesosphere as diagnosed from microwave limb sounder data, *J. Atmos. Sci.*, **53**, 217–240, 1996.
- Garcia, R. R., and S. Solomon, A new numerical model of the middle atmosphere, 2, Ozone and related species, *J. Geophys. Res.*, **99**, 12,937–12,951, 1994.
- Garcia, R. R., F. Stordal, S. Solomon, and J. T. Kiehl, A new numerical model of the middle atmosphere, 1, Dynamics and transport of tropospheric source gases, *J. Geophys. Res.*, **97**, 12,967–12,991, 1992.
- Hall, T. M., and R. A. Plumb, Age as a diagnostic of stratospheric transport, *J. Geophys. Res.*, **99**, 1059–1070, 1994.
- Hall, T. M., and M. J. Prather, Simulations of the trend and annual cycle in stratospheric CO₂, *J. Geophys. Res.*, **98**, 10,573–10,581, 1993.
- Hall, T. M., and M. J. Prather, Seasonal evolutions of N₂O, O₃, and CO₂: Three-dimensional simulations of stratospheric correlations, *J. Geophys. Res.*, **100**, 16,699–16,720, 1995.
- Hall, T. M., and D. W. Waugh, Timescales for the stratospheric circulation derived from tracers, *J. Geophys. Res.*, **102**, 8991–9001, 1997a.
- Hall, T. M., and D. W. Waugh, Tracer transport in the tropical stratosphere due to vertical diffusion and horizontal mixing, *Geophys. Res. Lett.*, **24**, 1383–1386, 1997b.
- Hall, T. M., and D. W. Waugh, The influence of nonlocal chemistry on tracer distributions: Inferring the mean age of air from SF₆, *J. Geophys. Res.*, **103**, 13,327–13,336, 1998.
- Hannegan, B., S. Olsen, M. Prather, and X. Zhu, The dry stratosphere: A limit on cometary water influx, *Geophys. Res. Lett.*, **25**, 1649–1652, 1998.
- Harnisch, J., R. Borchers, P. Fabian, and M. Maiss, Tropospheric trends for CF₄ and C₂F₆ since 1982 derived from SF₆ dated stratospheric air, *Geophys. Res. Lett.*, **23**, 1099–1102, 1996.
- Jackman, C. H., P. A. Newman, P. D. Guthrie, and M. R. Schoeberl, Effects of computed horizontal diffusion coefficients on two-dimensional N₂O model distributions, *J. Geophys. Res.*, **93**, 5213–5219, 1988.
- Jackman, C. H., E. L. Fleming, S. Chandra, D. B. Conditine, and J. E. Rosenfield, Past, present, and future modeled ozone trends with comparisons to observed trends, *J. Geophys. Res.*, **101**, 28,753–28,767, 1996.
- Jones, D. B. A., H. R. Schneider, and M. B. McElroy, Effects of the quasi-biennial oscillation on the zonally averaged transport of tracers, *J. Geophys. Res.*, **103**, 11,235–11,249, 1998.
- Jost, H., M. Loewenstein, L. Pfister, J. J. Margitan, A. Y. Chang, R. J. Salawitch, and H. A. Michelsen, Filaments in the tropical middle atmosphere: Origin and age estimation, *Geophys. Res. Lett.*, **25**, 4337–4340, 1998.
- Kida, H., General circulation of air parcels and transport characteristics derived from a hemispheric GCM, 2, Very long-term motions of air parcels in the troposphere and stratosphere, *J. Meteorol. Soc. Jpn.*, **61**, 510–522, 1983.
- Ko, M. K. W., K. K. Tung, D. K. Weisenstein, and N. D. Sze, A zonal mean model of stratospheric tracer transport in isentropic coordinates: Numerical simulations for nitrous oxide and nitric acid, *J. Geophys. Res.*, **90**, 2313–2329, 1985.
- Lin, S. J., and R. B. Rood, Multidimensional flux-form semi-Lagrangian transport schemes, *Mon. Weather Rev.*, **124**, 2046–2070, 1996.
- Maiss, M., L. P. Steele, R. J. Francey, P. J. Fraser, R. L. Langenfelds, N. B. A. Trivett, and I. Levin, Sulfer hexafluoride: A powerful new atmospheric tracer, *Atmos. Environ.*, **30**, 1621–1629, 1996.
- Minschwaner, K., A. E. Dessler, J. W. Elkins, C. M. Volk, D. W. Fahey, M. Loewenstein, J. R. Podolske, A. E. Roche, and K. R. Chan, The bulk properties of isentropic mixing into the tropics in the lower stratosphere, *J. Geophys. Res.*, **101**, 9433–9439, 1996.
- Mote, P. W., K. H. Rosenlof, M. E. McIntyre, E. S. Carr, J. C. Gille, J. R. Holton, J. S. Kinnnersley, H. C. Pumphrey, J. M. Russell, and J. W. Waters, An atmospheric tape recorder: The imprint of tropical tropopause temperatures on stratospheric water vapor, *J. Geophys. Res.*, **101**, 3989–4006, 1996.
- Mote, P. W., T. J. Dunkerton, M. E. McIntyre, E. A. Ray, and P. H. Haynes, Vertical velocity, vertical diffusion, and dilution by midlatitude air in the tropical lower stratosphere, *J. Geophys. Res.*, **103**, 8651–8666, 1998.

- Neu, J. L., and R. A. Plumb, The age of air in a leaky pipe model of stratospheric transport, *J. Geophys. Res.*, in press, 1999.
- Park, J., et al., The Atmospheric Effects of Stratospheric Aircraft: Reports of the 1998 Models and Measurements II Workshop, *NASA Tech. Publ.*, in press, 1999.
- Patra, P. K., S. Lal, B. H. Subbaraya, C. H. Jackman, and P. Rajaratnam, Observed vertical profile of sulphur hexafluoride (SF_6) and its atmospheric applications, *J. Geophys. Res.*, *102*, 8855–8859, 1997.
- Pitari, G., V. Rizi, L. Ricciardulli, and G. Visconti, High-speed civil transport impact: Role of sulfate, nitric acid trihydrate, and ice aerosols studied with a two-dimensional model including aerosol physics, *J. Geophys. Res.*, *98*, 23,141–23,164, 1993.
- Plumb, R. A., A tropical pipe model of stratospheric transport, *J. Geophys. Res.*, *101*, 3957–3972, 1996.
- Plumb, R. A., and M. K. W. Ko, Interrelationships between mixing ratios of long-lived stratospheric constituents, *J. Geophys. Res.*, *97*, 10,145–10,156, 1992.
- Plumb, R. A., and D. D. McConalogue, On the meridional structure of long-lived stratospheric constituents, *J. Geophys. Res.*, *93*, 15,897–15,913, 1988.
- Politowicz, P. A., and M. H. Hitchman, Exploring the effects of forcing quasi-biennial oscillations in a two-dimensional model, *J. Geophys. Res.*, *102*, 16,481–16,497, 1997.
- Prather, M. J., Numerical advection by conservation of second-order moments, *J. Geophys. Res.*, *91*, 6671–6681, 1986.
- Prather, M. J., and E. Remsberg, The Atmospheric Effects of Stratospheric Aircraft: Reports of the 1992 Models and Measurements Workshop, *NASA Ref. Publ.*, *1292*, 1993.
- Prather, M. J., M. B. McElroy, S. C. Wofsy, G. Russell, and D. Rind, Chemistry of the global troposphere: Fluorocarbons as tracers of air motion, *J. Geophys. Res.*, *92*, 6579–6613, 1987.
- Randel, W. J., B. A. Boville, J. C. Gille, P. L. Bailey, S. T. Massie, J. B. Kumer, J. L. Mergenthaler, and A. E. Roche, Simulation of stratospheric N_2O in the NCAR CCM2: Comparison with CLAES data and global budget analysis, *J. Atmos. Sci.*, *51*, 2834–2845, 1994.
- Randel, W. J., F. Wu, J. M. Russell, A. Roche, and J. W. Waters, Seasonal cycles and QBO variations in stratospheric CH_4 and H_2O observed in UARS HALOE data, *J. Atmos. Sci.*, *55*, 163–184, 1998.
- Randeniya, L. K., P. F. Vohralik, I. C. Plumb, and K. R. Ryan, Heterogeneous BrONO_2 hydrolysis: Effect on NO_2 columns and ozone at high latitudes in summer, *J. Geophys. Res.*, *102*, 23,543–23,557, 1997.
- Rasch, P. J., Conservative shape-preserving two-dimensional transport on a spherical reduced grid, *Mon. Weather Rev.*, *122*, 1337–1350, 1994.
- Rasch, P. J., B. A. Boville, and G. P. Brasseur, A three-dimensional general circulation model with coupled chemistry for the middle atmosphere, *J. Geophys. Res.*, *100*, 9041–9071, 1995.
- Rind, D., R. Suozzo, N. K. Balachandran, A. Lacis, and G. Russell, The GISS global climate/middle atmosphere model, I, Model structure and climatology, *J. Atmos. Sci.*, *45*, 329–370, 1988.
- Rind, D., D. Shindell, P. Lonergan, and N. K. Balachandran, Climate change and the middle atmosphere, III, The doubled CO_2 climate revisited, *J. Clim.*, *11*, 876–894, 1998.
- Rosenfeld, J. E., D. B. Considine, P. E. Meade, J. T. Bacmeister, C. H. Jackman, and M. R. Schoeberl, Stratospheric effects of Mount Pinatubo aerosol studied with a coupled two-dimensional model, *J. Geophys. Res.*, *102*, 3649–3670, 1997.
- Rosenlof, K. H., Seasonal cycle of the residual mean circulation in the stratosphere, *J. Geophys. Res.*, *100*, 5173–5191, 1995.
- Schmidt, U., and A. Khedim, In situ measurements of carbon dioxide in the winter arctic vortex and at midlatitudes: An indicator of the age of stratospheric air, *Geophys. Res. Lett.*, *18*, 763–766, 1991.
- Shia, R. L., M. K. W. Ko, D. K. Weisenstein, C. Scott, and J. Rodriguez, Transport between the tropical and midlatitude lower stratosphere: Implications for ozone response to high-speed civil transport emissions, *J. Geophys. Res.*, *103*, 25,435–25,446, 1998.
- Smyshlyaev, S. P., V. L. Dvortsov, M. A. Geller, and V. A. Yudin, A two-dimensional model with input parameters from a GCM: Ozone sensitivity to different formulation for the longitudinal temperature variation, *J. Geophys. Res.*, *103*, 28,373–28,387, 1998.
- Vohralik, P. F., L. K. Randeniya, I. C. Plumb, and K. R. Ryan, Use of correlations between long-lived atmospheric species in assessment studies, *J. Geophys. Res.*, *103*, 3611–3627, 1998.
- Volk, C. M., et al., Quantifying transport between the tropical and mid-latitude lower stratosphere, *Science*, *272*, 1763–1768, 1996.
- Volk, C. M., J. W. Elkins, D. W. Fahey, G. S. Dutton, J. M. Gilligan, M. Lowenstein, P. R. Podolske, K. R. Chan, and M. R. Gunson, Evaluation of source gas lifetimes from stratospheric observations, *J. Geophys. Res.*, *102*, 25,543–25,564, 1997.
- Waugh, D. W., et al., Three-dimensional simulations of long-lived tracers using winds from MACCM2, *J. Geophys. Res.*, *102*, 21,493–21,513, 1997.
- Woodbridge, E. L., et al., Estimates of total organic and inorganic chlorine in the lower stratosphere from in situ and flask measurements during AASE II, *J. Geophys. Res.*, *100*, 3057–3064, 1995.
- Yudin, V. A., S. P. Smyshlyaev, M. A. Geller, and V. L. Dvortsov, Transport diagnostics of GCMs and implications for 2D chemistry-transport model of troposphere and stratosphere, *J. Atmos. Sci.*, in press, 1999.
- Zubov, V. A., I. L. Karol, Y. E. Ozolin, and E. V. Rozanov, The zonally-averaged model of the photochemical, radiative and dynamical processes in the troposphere and stratosphere, 1, The description of the model and model validation, *Phys. Atmos. Ocean*, *31*, 1995.
- Zubov, V. A., E. V. Rozanov, and M. Schlesinger, Hybrid scheme for Three-dimensional advective transport, *Mon. Weather Rev.*, *127*, 1335–1346, 1999.

K. A. Boering, Department of Chemistry, University of California, Berkeley, CA 94720. (boering@cchem.berkeley.edu)

T. M. Hall, NASA Goddard Institute for Space Studies, 2880 Broadway, New York, NY 10025. (thall@giss.nasa.gov)

R. A. Plumb, Department of Earth, Atmosphere, and Planetary Science, Massachusetts Institute of Technology, Cambridge, MA 02139. (rap@rossby.mit.edu)

D. W. Waugh, Department of Earth and Planetary Science, Johns Hopkins University, 3400 North Charles Street, Baltimore, MD 21218. (waugh@jhu.edu)

(Received August 6, 1998; revised April 2, 1999; accepted April 7, 1999.)